Intermolecular Interactions and Local Density Augmentation in Supercritical Solvation: A Survey of Simulation and Experimental Results

W. Song, R. Biswas, and M. Maroncelli*

Department of Chemistry, The Pennsylvania State University, University Park, Pennsylvania 16802

Received: March 7, 2000; In Final Form: May 4, 2000

Data from prior simulation and experimental studies (a total of 52 solute/solvent pairs) are collected and analyzed in an attempt to relate the extent of local density augmentation in supercritical fluids to the strength of intermolecular interactions. For this purpose, intermolecular potential functions consisting of pairwise additive atom−atom potentials, with parameters either taken from literature sources or derived from quantum chemical calculations, are constructed and tested against experimental second-pressure virial coefficient data. For the solute−solvent combinations of interest in supercritical systems near room temperature, such potentials are found to reproduce experimental second-pressure virial coefficient data with reasonable accuracy. On the basis of these potentials, a variety of characteristics of solute−solvent and solvent−solvent interactions are computed and compared to simulated and experimental measures of density augmentation. It is found that the extent of augmentation is strongly correlated to measures of the free energy of solute−solvent interaction. However, simulated and experimental augmentation data apparently follow distinct correlations with these free energies, indicating the presence of a widespread error in either the measurement or the interpretation of density augmentation in supercritical solvents.

I. Introduction

When a large polyatomic solute is dissolved in a near-critical solvent, the local environment it sees usually differs from that expected on the basis of bulk fluid properties. In highly compressible fluids, "attractive"[1] solutes induce a region of local solvent density that can be much greater than the density of the bulk solvent. This "local density augmentation" is manifest in many solute-centered observables, for example in the density-dependent shifts of electronic spectra. Such spectroscopic data indicate that at reduced temperatures $T/T_c < 1.1$ and densities $\rho/\rho_c \sim 0.6$, the apparent solvent density in the immediate vicinity of a solute may be 2−3 times that of the bulk fluid. Understanding this solute-induced density enhancement is of both fundamental interest and practical importance if one wants to use supercritical solvents for any of a variety of common applications.[2,3]

Despite plentiful research over the past decade,[4−6] a complete understanding of local density augmentation has yet to be achieved. One unresolved question is the way in which the phenomenon is linked to solvent criticality. The divergence of solute partial molar volumes near a solvent's critical point—the observation that first aroused interest in the unique features of supercritical solvation[7,8]—has clearly been demonstrated to result from the long-range density fluctuations characteristic of near-critical fluids.[9−13] However, the relevance of long-range correlations to the local environment actually sensed by most solute-centered observables is a matter still open for debate.[12−14] The simple models currently used to interpret experiments completely ignore such fluctuations, focussing instead on the strength of solute−solvent interactions.[15−17] Calculations on simple Lennard−Jones model systems[11,12,18−20] also point to the relative strength of solute−solvent versus solvent−solvent interactions as being the key determinant of the extent of density augmentation. However, local densities measured in experiments often show a surprising indifference to the details of solute−solvent interactions. For example, Sun and co-workers[21] noted that systems as diverse as the nonpolar solute pyrene and the highly polar probe "PRODAN" show similar behavior in several supercritical fluids. Recent studies of four substituted anthracenes in three supercritical solvents showed little, if any, variation in the apparent density augmentation deduced from electronic shifts, despite what would appear to be substantial differences in the strength and nature of the solute−solvent interactions present in the various systems.[22] Furthermore, the augmentation observed in these systems is also remarkably similar to that determined for completely unrelated solutes, for example di-*tert*-butyl nitroxide[23] and the highly dipolar solute coumarin-153.[24] This apparently "universal" behavior suggests that, at least beyond some threshold, the particulars of solute−solvent interactions might not be important for determining the local environment a solute induces in a supercritical solvent.

The present study, motivated by the above observations, is an empirical look at the connection between density augmentation and intermolecular interactions.[25] For this purpose, we have collected data on 52 diverse solute/solvent combinations from prior simulation[19,26−33] and experimental studies.[21−26,34−45] We assume that the key features of the solute−solvent and/or solvent−solvent interactions of relevance are captured in the interactions between only two molecules at a time. Using pairwise additive all-atom potential functions, we compute various measures of the strength of solute−solvent and solvent−solvent interactions in these systems and correlate them to the observed extent of density augmentation. We find that there is, in fact, a clear relationship between density augmentation and measures of the free energy of solute−solvent association in both simulated and experimental systems. The uniform behavior

* Author to whom correspondence should be addressed.

10.1021/jp000888d CCC: $19.00
Published on Web 07/06/2000

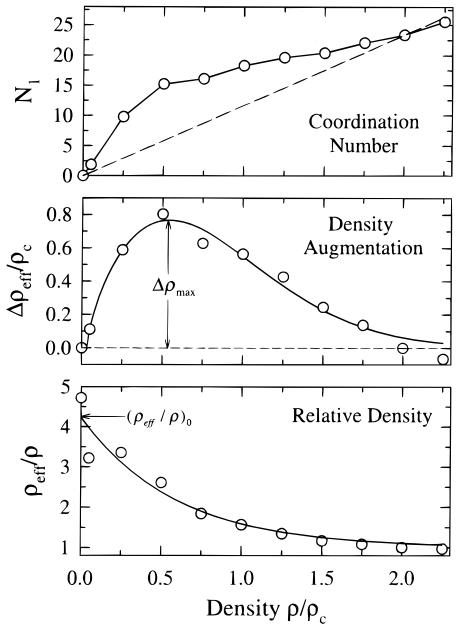

Figure 1. Typical data from simulations of coumarin-153 in ethane (T = 310 K)[33] used to illustrate the measures of local densities employed. The top panel shows coordination numbers N_1, the number of solvent molecules contained within the (nonspherical) first coordination shell of the solute, versus bulk solvent density ρ. The dashed line in this panel shows the use of a reference density, $\rho_{ref} = 2\rho_c$, to define the behavior expected in the absence of augmentation. The bottom two panels show the two measures of effective density described in the text.

noted in some experimental studies appears to reflect mainly the relatively narrow range of these free energies covered by many of the apparently diverse systems mentioned above. An unexpected result of the present study is the observation of a systematic difference between the extent of augmentation found in simulated systems and that found in experimental systems.

The remainder of this paper is structured as follows. In Section IIA we discuss how local densities and density augmentation are derived from simulation and experimental data. In Section IIB we define various quantities used to characterize the interactions between isolated pairs of molecules. Section III contains a discussion of the intermolecular potential functions used in these calculations, along with a comparison of calculated and experimental second-pressure virial coefficients, undertaken as a test of the potentials' accuracy. In Sections IV and V we present the collected data on local densities in supercritical fluids and correlate it to an assortment of characteristics of the binary interactions between solute−solvent and solvent−solvent pairs. Finally, the main results of this work are summarized and further interpreted in Section VI.

II. Analysis Methods

A. Measures of Effective Local Densities. It is important to begin our discussion by defining what we mean by local density, and how it is measured in simulation and experiment.[46] The situation is simplest in the case of computer simulation, where density can be directly monitored. Here one can define local densities in terms of the average numbers of solvent molecules (or atoms) found within a given region surrounding the solute. An example of typical simulation data is provided in Figure 1. These data are from molecular dynamics simulations of the solute coumarin-153 in supercritical ethane (T/T_c = 1.02).[33] Shown in the top panel are the numbers of solvent molecules in the first solvation shell of the solute, plotted as a function of the bulk density ρ. All that is needed to convert these coordination numbers into local densities is a normalization constant.

There are two ways of defining this normalization constant. The first is to use the volume of the solvation shell considered. Such a definition produces true local densities and it is unambiguous, except for some freedom in the choice of volume excluded by the solute. However, local densities defined in this manner tend to be about 2−3 times higher than bulk densities under liquidlike conditions ($T \cong T_c$ and $\rho \geq 2\rho_c$) as a result of packing constraints.[47] If one wants to focus attention on density enhancements resulting from attractive interactions in the near-critical regime, it is desirable to remove this structural effect. We therefore choose an alternative definition of the proportionality so that the local density becomes equal to the bulk density at some high-density reference state where one expects attractive interactions to have a negligible effect on the structure. Specifically, we define *effective* local densities from simulated coordination numbers using the relation

$$\rho_{eff}(\rho) \equiv N_1(\rho)\left(\frac{\rho}{N_1}\right)\rho_{ref} \tag{1}$$

and we take as a reference state $\rho_{ref} = 2\rho_c$.

Some comment is necessary concerning the choice of reference density $\rho_{ref} = 2\rho_c$, because this choice has a nonnegligible effect on the values of ρ_{eff} we report. Although there is no unique way to choose ρ_{ref}, it might seem most logical to employ a value typical of the densities of the liquid solvents to which supercritical solvents are usually compared, i.e., a density of between 2.5 and $3.0\rho_c$. We choose a value shy of this liquid range for the simple reason that supercritical data are usually not available for densities higher than $\sim 2\rho_c$.[48] The quantitative effect of using a reference value of $2\rho_c$ rather than, say, $2.75\rho_c$ can be estimated using available data from simulations on Lennard−Jones solutes and solvents.[19] Based on such data, we anticipate that the maximum augmentation values might be smaller than values obtained with the higher density reference by as much as 20%, whereas the limiting enhancement factors should be little affected.

Given this definition of effective densities, we use two further functions, the *augmentation* $\Delta\rho_{eff} \equiv \rho_{eff} - \rho$ and the *enhancement factor* ρ_{eff}/ρ, illustrated in Figure 1, to measure how the local and bulk densities differ in a given system. The density augmentation $\Delta\rho_{eff}$ vanishes at both $\rho = 0$ and ρ_{ref}, and is maximal between these points, typically near a density of $0.6\rho_c$ (see Section IV). To characterize the dependence of $\Delta\rho_{eff}$ on bulk density, it is convenient to fit simulated or experimental data to a Weibull line shape function

$$\Delta\rho_{eff} = a\left(\frac{c-1}{c}\right)^{(1-c)/c}\left[\frac{\rho-\rho_0}{b} + \left(\frac{c-1}{c}\right)^{1/c}\right]^{c-1}\exp\left\{-\left[\frac{\rho-\rho_0}{b} + \left(\frac{c-1}{c}\right)^{1/c}\right]^c + \frac{c-1}{c}\right\} \tag{2}$$

An example of such a fit is shown as the smooth curve in the middle panel of Figure 1. Although there is no theoretical justification for this functional form, it provides a good representation of the density dependence observed in most of the data sets examined. We therefore use the maximum value obtained from such fits "$\Delta\rho_{max}$" as one measure of the extent of augmentation. A second measure comes from enhancement factors ρ_{eff}/ρ such as those shown on the bottom panel of Figure 1. In most cases, especially where the augmentation is large, ρ_{eff}/ρ appears to increase monotonically with decreasing density.

(For experimental examples, see Figure 4 and the data in refs 22 and 24.) As shown by the smooth curve through the points in Figure 1, an exponential function,

$$\rho_{\text{eff}}/\rho = 1 + a\exp(-b\rho) \tag{3}$$

fits the data reasonably. We use such fits to extrapolate ρ_{eff}/ρ versus ρ to zero density "$(\rho_{\text{eff}}/\rho)_0$" and use this value as a second measure for comparison. However, ρ_{eff}/ρ need not be monotonic in ρ, and some data sets we have examined appear to show a maximum at low but nonzero densities. In these cases we use the maximum value of ρ_{eff}/ρ in place of the extrapolated value as the second, semi-independent measure of the extent of augmentation in a given system.

Determining effective densities from experimental data involves one additional step compared to computer simulation. Rather than measuring density directly, in experiment one measures some solute-centered observable that is sensitive to local solvent properties, and thus local density, but only indirectly. To obtain densities one must know how the observable depends on solvent conditions, either on the basis of theoretical modeling or, more often, through calibrating the behavior of the observable in liquid solvents, where local and bulk properties are assumed to be "identical". As an example of translating typical experimental data into effective densities, consider frequency shifts of electronic spectra, one of the most common experimental observables. We have found that the frequencies of the electronic spectra of many chromophores in nonpolar liquid solvents can be predicted from the refractive index of the solvent (n) using the dielectric continuum expression[22,24,49]

$$\nu_{\text{el}} = \nu_0 + aR(n^2) \quad \text{where} \quad R(x) \equiv \frac{x-1}{x+2} \tag{4}$$

and ν_0 is the gas-phase frequency and a an empirical constant. If the relationship between refractive index (or $R(n^2)$) and density, $R = f(\rho)$, in a supercritical fluid is known, an effective local density can be deduced from the observed spectral shift via

$$\rho_{\text{eff}}{}^{\nu} \equiv f^{-1}\{R_{\text{eff}} = (\nu_{\text{obs}} - \nu_0)/a\} \tag{5}$$

In the supercritical fluids of interest here the reaction field factor $R(n^2)$ is proportional to density,[22] so that, in fact, the relation between the spectral shift and density is simply $\rho_{\text{eff}}{}^{\nu} \propto (\nu_{\text{obs}} - \nu_0)$.[50] For other observables—for example, vibrational relaxation or dephasing rates—such a simple relationship may or may not exist. In either case, it is important to recognize that the local densities measured from experiment can be only as accurate as one's knowledge of the connection between the observable used for measurement and local density. This connection is never known with complete certainty.

B. Calculation of Solute−Solvent Interaction Parameters. In this work we assume that the main determinants of local densities in supercritical fluids derive from the intermolecular potential between the solute and solvent in question. For each of the systems examined, we therefore seek to characterize this potential by calculating various averages over the interactions between isolated solvent−solute pairs. (Similar calculations for solvent−solvent pairs are also performed for comparison purposes.) These calculations are carried out using the intermolecular potentials described in the following section and a simple Monte Carlo sampling strategy. For a given pair of molecules, one is defined to be the solute (u) and the other the solvent (v). The solute's center of mass is fixed at the origin, and various properties related to the solute−solvent interaction are sampled as the position and orientation of the solvent molecule are varied. The sampling is carried out such that the accuracy in the computed quantities is expected to be better than ±5% in all cases.

TABLE 1: Primary Characteristics of the Pair Potentials Examined

observable	meaning
V_{ij} (V_{vv}, V_{uv})	excluded volume of ij pair (eq 6)
V_{i0} (V_{u0})	effective volume of species i (eq 6)
B_{ij} (B_{uv}, B_{vv})	second virial coefficient between i and j (eq 7)
K_{ij} (K_{uv}, K_{vv})	$i-j$ association constant (eq 10) and free energy ΔG_{ij} (eq 11)
U_{ij} (U_{uv}, U_{vv})	"solvation energy" per solvent molecule ((U_{ij}/ρ_j) eq 12)
α_{ij} (α_{uv}, α_{vv})	average free energy of j in first solvation shell of i (depth of $a_\Omega(s)$; eq 14)
ϵ_{ij} (ϵ_{uv}, ϵ_{vv})	average potential of j in first solvation shell of i (depth of $u_\Omega(s)$; eq 15)

For the polyatomic solutes and solvents of interest here, it is far from obvious just what the most important features of the solute−solvent interaction might be, or indeed how to measure them. For this reason we have calculated a variety of volumetric and energetic parameters in order to examine their correlations with measures of local densities. All of these parameters are based on the primary properties listed in Table 1. The first five entries in Table 1 involve integrations of angle-averaged quantities over the center of mass separation between the solute and solvent, r. The simplest are the pair excluded volumes V_{ij}, which we define by

$$V_{ij} = 4\pi\int_0^\infty \langle\Theta[u_{ij}^{\text{LJ}}(r,\vec{\Omega})]\rangle_{\vec{\Omega}} r^2 \mathrm{d}r \tag{6}$$

where $\Theta(x)$ is the step function $\Theta(x) = 0$ for $x < 0$ and $\Theta(x) = 1$ for $x \geq 0$, and u_{ij}^{LJ} denotes the Lennard−Jones component of the interaction between molecules i and j (see eq 16). The angular variables symbolized by $\vec{\Omega}$ include both the orientation of the solvent molecule (0, 2, or 3 angles) plus the two angles locating its center of mass on a sphere of radius r about the solute. The notation $\langle x\rangle_{\vec{\Omega}}$ signifies an average over random samples of all of these angles. The species volumes V_{i0} are defined analogously to V_{ij}, but with a vanishingly small test particle "0" replacing j. Both of these volumes are temperature-independent. They are used to measure the relative sizes of solute and solvent molecules and to estimate the number of solvent molecules in the first solvation shell of the solute. (See Section IV.)

The remaining properties in Table 1 are thermal averages used to gauge the strength of solute−solvent interactions. The second-pressure virial coefficients are defined in the usual manner:[51]

$$B_{ij} = -2\pi\int_0^\infty \langle\exp\{-u_{ij}(r,\vec{\Omega})/k_{\text{B}}T\} - 1\rangle_{\vec{\Omega}} r^2 \mathrm{d}r \tag{7}$$

with $u_{ij}(r,\vec{\Omega})$ being the total interaction potential between i and j. This relation can also be expressed

$$B_{ij} = -2\pi\int_0^\infty \{g_{ij}{}^0(r) - 1\} r^2 \mathrm{d}r \tag{8}$$

where the angle-averaged Boltzmann factor

$$g_{ij}{}^0(r) \equiv \langle\exp\{-u(r,\vec{\Omega})/k_{\text{B}}T\}\rangle_{\vec{\Omega}} \tag{9}$$

is the equivalent of the radial distribution function for a pair of

spherically symmetric molecules in the zero-density limit (denoted by the "0" superscript). That is, $4\pi r^2 g_{ij}^0(r)$ is the relative probability of molecules *i* and *j* being found separated by a distance *r*, independent of their orientation. For pairs containing at least one large molecule, B_{ij} measures some sort of "attractive volume" associated with the *i*−*j* pair. The main impetus for calculating this particular characteristic of the intermolecular potential is that it can be measured experimentally. In section III we use the data available on the solvents and solutes of interest to assess the accuracy of our interaction models.

A similar integral over $g_{ij}^0(r)$, which might be expected to be more closely related to density augmentation, is the association constant

$$K_{ij} = 4\pi \int_0^{R_c} g_{ij}^0(r) r^2 \mathrm{d}r \tag{10}$$

Apart from the neglect of intramolecular effects, this quantity represents the equilibrium constant for the gas-phase association process $i + j \rightarrow (ij)$.[52] The cutoff radius R_c specifies the region over which the *i*−*j* pair is deemed "associated". The choice of cutoff is somewhat arbitrary, but the relative magnitudes of K_{ij} for different solute−solvent pairs are insensitive to the particular value chosen within a reasonable range. Here we define R_c to be the radius beyond which $g_{ij}^0(r)$ falls below the value 2.[53] Like B_{ij}, the association constant is a Boltzmann weighted volume of the *ij* pair. Its logarithm is the free energy of association

$$\Delta G_{ij} = -k_B T \ln K_{ij} \tag{11}$$

The final integral quantity, U_{ij}, defined by[54]

$$U_{ij}/\rho_j = 4\pi \int_0^{\infty} \langle \exp\{-u(r,\vec{\Omega})/k_B T\} u(r,\vec{\Omega}) \rangle_{\vec{\Omega}} r^2 \mathrm{d}r \tag{12}$$

provides an estimate of the "solvation energy" of the solute *i* in the solvent *j*. Specifically, U_{ij} would describe the net interaction energy between a solute *i* and solvent comprising of molecules *j* if the relative probability of a solvent molecule having relative coordinates $(r,\vec{\Omega})$ was given by the Boltzmann factor $\exp\{-u(r,\vec{\Omega})/k_B T\}$.[54] Because this Boltzmann factor is correct only in the $\rho_j \rightarrow 0$ limit, eq 12 does not actually provide the solvation energy that would be found in a dense solvent of *j* molecules. Nevertheless, U_{ij}/ρ_j is a distinct characteristic of the solvation energetics that should be useful for relative comparison.

We also examine two other properties which provide estimates of the energetics of a solvent molecule within the first solvation shell of the solute. To define these properties, we first digress to discuss the "solvation shell distribution function"

$$g_{ij}^{ss}(s) \equiv \langle \exp\{-u(s,\vec{\Omega})/k_B T\} \rangle_{s(\vec{\Omega},r)} \tag{13}$$

This distribution function differs from $g_{ij}(r)$ defined in eq 9 only in that the distribution variable *s* is now the distance between the center of mass of molecule *j* (the "solvent") and the *nearest atom of the solute i*. (The subscript "$s(\vec{\Omega}, r)$"signifies that averaging is performed over all combinations of both the center of mass distance *r* and orientation variables $\vec{\Omega}$, consistent with a given value of *s*.) The greater utility of $g_{ij}^{ss}(s)$ compared to $g_{ij}(r)$ is illustrated in Figure 2a, using representative data for the pyrene−CO_2 pair. Pyrene is typical of many of the solutes studied here in that its shape is far from spherical. For this reason, center-of-mass distribution functions are of little value in revealing its solvation structure. Note, for example, that $g_{ij}(r)$ in Figure 2a is quite broad and even exhibits a secondary peak as a result of pyrene atoms being distributed over a range of distances from its center of mass. The alternative choice of nearest-solute-atom distances *s* minimizes the broadening and extraneous structure and produces distributions analogous to those observed for spherical potentials.[55] These $g_{ij}^{ss}(s)$ functions provide the best indicator of the relative probability of finding a solvent molecule within the first solvation shell of the solute.

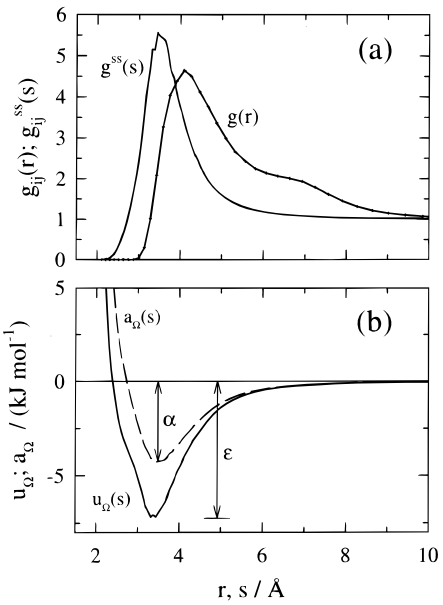

Figure 2. Computed distribution functions and energies calculated for the system pyrene/CO_2. The top panel illustrates the difference between the distribution function $g_{ij}(r)$ defined in terms of the center-of-mass separation and the "solvation-shell distribution function" defined in terms of the distance *s* from the center of mass of the solute molecule to the nearest atom of the solvent. The bottom panel shows the potential $u_\Omega(s)$ and free-energy $a_\Omega(s)$ functions derived from $g_{ij}^{ss}(s)$ according to eqs 14 and 15.

The characteristic energy parameter α_{ij} is a measure of this probability, described as a relative free energy. That is, we transform $g_{ij}^{ss}(s)$ into the equivalent free-energy function

$$a_\Omega(s) = -k_B T \ln g_{ij}^{ss}(s) \tag{14}$$

and define α_{ij} to be the depth of the $a_\Omega(s)$ well. Note that $a_\Omega(s)$ is a free energy rather than a potential energy by virtue of the averaging over the solvent and solute orientational degrees of freedom (indicated by the Ω subscript). The parameter α_{ij} can be viewed as the free-energy benefit a solvent molecule receives by being in the first solvation shell of the solute (at least in the limit of zero solvent density). Corresponding to $a_\Omega(s)$, we can also define the orientationally averaged potential energy by

$$u_\Omega(s) = \frac{\langle u(r,\vec{\Omega}) \exp\{-u(r,\vec{\Omega})/k_B T\} \rangle_{s(\vec{\Omega},r)}}{\langle \exp\{-u(r,\vec{\Omega})/k_B T\} \rangle_{s(\vec{\Omega},r)}} \tag{15}$$

The final parameter in Table 1, ϵ_{ij}, specifies the depth of this potential energy well and can be similarly viewed as the energetic benefit of being in the first solvation shell. A comparison of these two functions for the pyrene−CO_2 pair is shown in Figure 2b. As illustrated here, it is a general result that $a_\Omega(s) \geq u_\Omega(s)$. This inequality reflects the unfavorable entropy of association that derives from the loss of orientational freedom of the solute and solvent molecules near contact.

TABLE 2: Solvent Potentials Employed

molecule	T_c[a]/K	ρ_c[a]/mol dm^{-3}	error[b] in T_c	error[b] in ρ_c	notes	ref
C_2H_6	305.4	6.74	+0.9%	−2%	"TraPPE-EH" model	*f*
C_3H_8	369.8	4.93	+0.5%	−4%	"TraPPE-EH" model	*f*
CO_2	304.1	10.6	0[c]	0[c]	"EPM2" model	*g*
SF_6	318.7	5.03	*d*	*d*	"6CLJ" (off-atom F sites)	*h*
CHF_3	299.3	7.54	< + 3%[e]	< + 19%[e]	modified from Potter et al.[e]	*i*
CH_3OH[c]	512.6	8.47	−0.1%	+2%	(united atom CH_3 group)	*j*
H_2O	647.3	17.5	−1%	−9%	SPC/E[k] model	*l*

[a] Experimental critical temperature and density taken from Reid, R. C.; Prausnitz, J. M.; Poling, B. E. *The Properties of Gases and Liquids*, 4th ed.; McGraw-Hill: New York, 1987. [b] $\{X(\text{clc}) - X(\text{obs})\}/X(\text{obs})$. [c] The potential was scaled so as to reproduce the experimental critical parameters to within the uncertainties in the simulations. [d] PVT data in the region of the critical point was fitted accurately, but the critical point of the model was not determined. [e] The original potential of ref 4 employed an H−F interaction that did not conform to the mixing rules of eq 17. We therefore rescaled the parameters from the original ones in order to use these mixing rules and also to better predict the critical properties. The parameters used (σ, ϵ/k_B, q) were the following: C(3.336 Å, 52.85 K, 0.4329 e), H(1.721 Å, 12.10 K, 0.1043 e), and F(3.151 Å, 38.72 K, −0.1791e). The critical point of this revised model was not determined; the values listed are the errors in the original model. [f] Chen, B.; Siepmann, J. I. *J. Phys. Chem. B* **1999**, *103*, 5370. [g] Harris, J. G.; Yung, K. H. *J. Phys. Chem.* **1995**, *99*, 12021. [h] Lustig, R. *Ber. Bunsen. Phys. Chem.* **1995**, *99*, 1462. [i] Potter, S.; Tildesley, D.; Burgess, A.; Rogers, S. *Mol. Phys.* **1997**, *92*, 825. [j] van Leeuwen, M. E.; Smit, B. *J. Phys. Chem.* **1995**, *99*, 1831. [k] Berendsen, H. J. C.; Grigera, J. R.; Straatsma, T. P. *J. Phys. Chem.* **1987**, *91*, 6269. [l] Guissani, Y.; Guillot, B. *J. Chem. Phys.* **1993**, *98*, 8221.

III. Intermolecular Potential Functions and Their Accuracy

To model intermolecular interactions, we adopt pairwise additive effective potentials of the sort commonly employed in computer simulation. Specifically, the interaction between two molecules *i* and *j* is assumed to be given by the sum of site−site terms of the Lennard−Jones plus Coulomb form

$$u_{ij} = \sum_{\alpha_i} \sum_{\beta_j} u_{\alpha\beta}(r_{\alpha\beta})$$

$$u_{\alpha\beta}(r_{\alpha\beta}) = 4\epsilon_{\alpha\beta}\left\{\left(\frac{\sigma_{\alpha\beta}}{r_{\alpha\beta}}\right)^{12} - \left(\frac{\sigma_{\alpha\beta}}{r_{\alpha\beta}}\right)^{6}\right\} + \frac{q_\alpha q_\beta}{r_{\alpha\beta}} \qquad (16)$$

where α and β label interaction sites on molecules *i* and *j*, respectively. In all cases, the parameters of unlike sites ($\alpha \neq \beta$) are obtained from like-atom parameters via the combining rules

$$\sigma_{\alpha\beta} = \frac{1}{2}(\sigma_{\alpha\alpha} + \sigma_{\beta\beta})$$

$$\epsilon_{\alpha\beta} = (\epsilon_{\alpha\alpha}\epsilon_{\beta\beta})^{1/2} \qquad (17)$$

Calculations for comparison to computer-simulated data use whatever potential functions and parameters were employed in the original simulations.[56] These simulation models often involve united-atom representations wherein multiple atoms are combined into a single interaction site. In fact, in many of the available simulation studies, both the solute and the solvent molecules are each represented by a single, uncharged Lennard−Jones site. In contrast, we use all-atom functions for comparison with experimental augmentation data. (The only exceptions involve the solvents methanol and methane.) Potential functions describing the supercritical solvents were taken mainly from literature sources, as listed in Table 2. Whenever possible, the potentials have been selected because they were parametrized to fit the liquid−vapor coexistence curve of the real fluid in the vicinity of its critical point. The accuracy of the critical temperatures and densities predicted by these potentials is noted in Table 2.

Solute molecules are modeled using a combination of semiempirical and ab initio calculations. The geometries employed are those found from an AM1 optimization at the Hartree−Fock level.[57] Charges are obtained from electrostatic potential fits to the 6-31G*/MP2 wave functions in the AM1 geometry.[58] Lennard−Jones parameters are taken from the OPLS all-atom parameter set optimized for condensed-phase simulation by Jorgensen and co-workers.[59,60] A listing of all geometries and potential parameters employed in these calculations is available as supplementary information to this article.

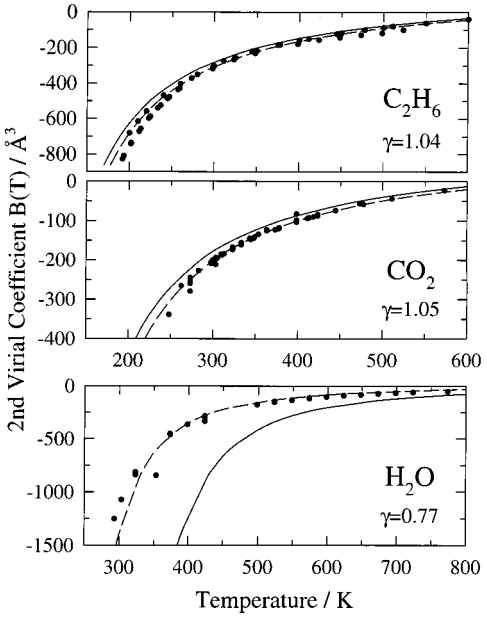

Figure 3. Comparison between experimental (filled circles; data from ref 61) and calculated second-pressure virial coefficients (solid curve). The dashed curve is the result of a temperature scaling $B_{\text{calc}}(T) \rightarrow B_{\text{calc}}(\gamma T)$ with the indicated values of the scale factor γ.

Before using these potential functions to explore the relationship between molecular interactions and density augmentation, it is important to consider how accurate they are likely to be. We do so by comparing second-pressure virial coefficients, $B_{ij}(T)$, calculated using these potentials to experimental values. Experimental virial data for many pure small-molecule fluids (i.e., $B_{ii}(T)$ data) are available over wide temperature ranges and have been conveniently summarized by Dymond and Smith.[61] Representative comparisons between calculated and observed data of this sort are illustrated in Figure 3, and a more complete comparison is provided in Table 3. The ethane and CO_2 examples shown in Figure 3 are typical of what is found for nondipolar solvents with potential parameters that have been fit to the solvent's critical properties: the calculated values of

TABLE 3: Observed and Calculated Second-Pressure Virial Coefficients

solute	solvent	system type[a]	T[b]/K	$-B_{obs}$[c]/Å^3	$-B_{calc}$/Å^3	B_{obs}/B_{calc}	γ[d]
Ar	Ar	VV	150	143	140	1.02	1.08
methane	methane	VV	200	178	145	1.23	1.09
CO_2	CO_2	VV	300	204	179	1.14	1.05
SF_6	SF_6	VV	300	459	377	1.22	1.10
ethane	ethane	VV	300	302	281	1.08	1.04
propane	propane	VV	300	634	578	1.10	1.04
CO_2	Ar	VV	275	82	83	0.99	
CO_2	methane	VV	289	104	97	1.07	
ethane	CO_2	VV	289	206	206	1.00	
						1.09 ± 0.09	*1.06 ± 0.04*[a]
fluoroform	fluoroform	pV	298	306	332	0.92	0.96
methanol	methanol	pL	523	260	310	0.84	0.96
water	water	pL	648	82	158	0.52	0.77
						0.76 ± 0.21	*0.90 ± 0.09*
benzene	benzene	LL	300	2424	1932	1.25	1.09
cyclohexane	cyclohexane	LL	310	2490	1879	1.32	
toluene	toluene	LL	374	2307	1693	1.36	1.10
chlorobenzene	chlorobenzene	LL	443	1607	1305	1.23	1.08
p-xylene	*p*-xylene	LL	375	3529	2557	1.38	1.09
cyclohexane	benzene	LL	361	1700	1261	1.35	
toluene	benzene	LL	453	1122	879	1.28	
						1.31 ± 0.06	*1.09 ± 0.01*
benzene	Ar	LV	318	168	198	0.85	
benzene	methane	LV	323	271	260	1.04	
benzene	CO_2	LV	306	447	528	0.85	~1.04
cyclohexane	Ar	LV	311	193	232	0.83	
cyclohexane	CO_2	LV	298	392	495	0.79	
naphthalene	Ar	SV	297	292	397	0.74	
naphthalene	methane	SV	294	603	569	1.06	0.97
naphthalene	CO_2	SV	297	951	1042	0.91	0.88
naphthalene	ethylene	SV	296	1106	1046	1.06	
naphthalene	ethane	SV	299	1202	1256	0.96	
phenanthrene	CO_2	SV	312	1177	1392	0.84	
phenanthrene	methane	SV	313	735	734	1.00	
phenanthrene	ethylene	SV	310	1467	1404	1.04	
anthracene	Ar	SV	348	304	401	0.76	
anthracene	methane	SV	339	541	600	0.90	0.97
anthracene	CO_2	SV	338	896	1105	0.81	0.93
anthracene	ethylene	SV	338	1139	1155	0.99	
anthracene	ethane	SV	336	1296	1469	0.88	0.95
anthracene	propane	SV	370	1441	1807	0.80	
anthracene	fluoroform	SV	298	1992	3127	0.64	
						0.90 ± 0.10	*0.96 ± 0.05*
water	Ar	pn	298	61.4	6.7	9.2	~1.3
water	methane	pn	298	104	17.9	5.8	~1.3
water	ethane	pn	298	207	42.9	4.8	~1.4
methanol	Ar	pn	298	144	77.3	1.9	~1.3
						(5 ± 3)	~1.3

[a] Most species are classified in terms of their state at room temperature and atmospheric pressure: V = vapor, L = liquid, S = solid, and p = polar. The final category pn, denotes unlike pairs with highly dissimilar like (*ii*) versus unlike (*ij*) interactions. [b] To the extent possible, temperatures for these comparisons are chosen either near 300 K or near to the critical point in the case of pure gases. [c] Most of the experimental data are from the compilations in Dymond, J.; Smith, E. *The Virial Coefficients of Pure Gases and Mixtures*; Clarendon Press: Oxford, 1980. The data for anthracene with propane and fluoroform are from Rossling, G. L.; Franck, E. U. *Ber. Bunsen.-Ges. Phys. Chem.* **1983**, *87*, 882. [d] γ is the temperature/energy scaling factor required to achieve the best agreement when scaling temperature-dependent virial coefficient data in the manner $B_{obs}(\gamma T) \cong B_{calc}(T)$. Whenever possible, γ was chosen to provide optimal agreement for $T \cong T_c$ in the case of pure fluids or $T = 300$ K in the case of mixed fluids.

$B_{ii}(T)$ are systematically too high, compared to experiment, by some 10−15%. However, excellent agreement with experimental values can be achieved through a temperature rescaling of the form $B_{obs}(\gamma T) = B_{calc}(T)$. The dashed curves in Figure 3 show the results of such scaling. In pure ethane and CO_2 the best scaling factors are found to be $\gamma = 1.04$ and 1.05, respectively. Scaling factors of other gases are listed in the top portion of Table 3. In general, we observe that for nonpolar or weakly polar gases, the required factors lie in the range $1.04 \leq \gamma \leq 1.10$.

Why should this sort of temperature adjustment be necessary? Scaling the temperature by γ is equivalent to requiring an overall rescaling of the pair potential by this same factor in order to achieve agreement with experiment. The direction and magnitude of this scaling are approximately what one would expect for simple nonpolar molecules, given the known differences between true pair potentials and the effective two-body potentials we use to represent them. When effective pair potentials of nonpolar species are parametrized to fit condensed-phase data, the net average repulsive contribution of many-body interactions present at high densities yields effective two-body potentials that are less attractive than the true two-body potential by some 5−15%.[62−65] Thus, the values of γ found here are of just the magnitude anticipated.

In the case of polar gases, exemplified by the water data in Figure 3, the situation is different. For this class of fluids, the

experimental virial coefficients are found to be less negative than the calculated values. As shown in Figure 3, the differences between B_{obs} and B_{calc} can become quite large at temperatures far below critical. However, here too, a relatively modest temperature scaling is able to bring the observed and calculated values into agreement. In the case of polar solvents, scaling factors of less than unity are required (Table 3). That a scaling in the opposite direction is found in these pure polar systems is also to be expected. In polar fluids, the three-body interactions of primary importance are inductive, rather than dispersive as in the nonpolar case. Accounting for the effects of induced electrical moments present in condensed phases through the use of effective pair potentials which lack explicit polarizability, requires charges 10−20% larger than those of the isolated molecule. Thus, one expects that to achieve agreement with experimental binary interaction data, the energy scale of the effective potential will have to be reduced slightly, just as indicated by these empirical γ factors.

The above comparisons would seem to indicate that the potential functions we employ represent the energies of interactions between isolated pairs of molecules to an accuracy of about ±10% in all but the water case. However, thus far we have only considered like-pair interactions between "solvent" molecules, molecules whose potential functions have been specifically parametrized to match coexistence properties of the pure fluid. What about pairs of unlike molecules, which constitute the solute/solvent combinations of primary interest here? Unfortunately, there is much less data available with which to test the accuracy of the interactions between disparate pairs. Because temperature-dependent data are limited, we mainly compare values of B_{obs} and B_{calc} at a single temperature. These comparisons are also summarized in Table 3, where we have organized pairs mainly according to the physical state (vapor, liquid, or solid) of the species at 300 K.

The top two groupings in Table 3, "VV" and "pp", mainly contain data on the pure supercritical solvents already discussed. The nondipolar liquid ("LL") systems display much the same behavior as the "VV" systems, except that they tend to underestimate the magnitude of B_{obs} by a greater amount: 31 ± 6% compared to 9 ± 9%. However, on the basis of limited temperature-dependent data, the scaling required in these cases ($\gamma \cong 1.09$) is found to be similar to that in the VV cases. The greater deviation in B for the "LL" set, therefore, does not necessarily reflect a less accurate representation of the intermolecular potentials of these molecules. Rather, it probably is due to the lower reduced temperatures (relative to T_c) at which $B(T)$ data are available.

The molecules grouped into the "LV, SV" set are most similar to the solute−solvent pairs for which extensive density augmentation data are available. For these molecules, the magnitude of $B(T)$ is slightly overestimated—on average by about 12%. The fact that the virial coefficients are reproduced to this accuracy is encouraging. It suggests that for the type of solute−solvent pairs of most interest here, the intermolecular potentials described above must at least capture the net "attractiveness" of the interactions reflected in $B(T)$ to roughly this same accuracy.

The final set of virial data are labeled "pn" to denote highly polar + nonpolar pairs. Such pairs represent a worst case for accurate modeling with the potential functions used here. For these combinations, the calculated virial coefficients are underestimated by factors of between 2 and 10 at room temperature. Such large errors appear to reflect underestimation of the true strength of the intermolecular interactions by some 30−40% (i.e., $\gamma \sim 1.3-1.4$). One can rationalize the direction and large magnitude of this discrepancy as once again resulting from neglect of explicit polarizability. The consequences of this neglect are particularly severe when a highly polar molecule such as water, which also has only weak dispersion interactions, is paired with a nonpolar molecule. A considerable fraction of the interaction energy in such a pair is expected to come from dipole-induced dipole interactions, absent in the effective potentials used. These last results are provided as a warning that the parameters calculated for systems involving water, and to a lesser extent those involving methanol, may contain substantial errors.

In light of all the above comparisons, we can summarize the anticipated accuracy of the characteristics derived from the potentials adopted here as follows. The relatively small uncertainties in geometries calculated using the AM1 method,[66] together with the success of OPLS potential parameters for reproducing liquid-state densities,[60] suggest that the volumetric properties or repulsive volumes (V_{ij}, V_{i0}) will be accurate to better than 5% in most cases. To gauge the relative attraction between pairs of molecules, we compute two types of quantities: those that depend "linearly" (α_{ij}, ϵ_{ij}, and ΔG_{ij}) and those that depend "exponentially" (B_{ij}, K_{ij}, and U_{ij}) on the pair potential. The temperature scaling noted above for virial coefficients suggests that the former quantities should be accurate to about ±10% (i.e., ±γ), at least in cases where strong electrostatic interactions are absent. In the presence of strong electrical interactions, much less virial data is available for calibration, but an accuracy of ±20% seems reasonable, except in cases involving water, where the errors may be larger. For the "exponential" quantities K_{ij} and U_{ij}, we expect accuracies on the same order as those observed for the B_{ij}, which we take to be ±30% in the nonpolar cases. For systems with strong electrical interactions, especially those involving water, estimates of the latter quantities could be in error by rather large amounts, and thus should be viewed with skepticism.

IV. Collected Augmentation Data

Tables 4 and 5 summarize data on local density augmentation collected from literature sources, together with characteristics of the solute−solvent and solvent−solvent interactions listed in Table 1. In collecting data for the present study, no attempt was made to be all-inclusive. Instead, we selected data believed to be both of high quality and amenable to the analysis discussed in Section II. Nevertheless, the results summarized in these tables should be representative of the full scope of this type of data currently available.

The simulations summarized in Table 4 constitute the majority of those reported to date which have analyzed density augmentation in near-critical systems.[67] (We do not include data on ions in supercritical water[68] because the interactions in such systems are rather distinct from those pertaining in other solute/fluid combinations.) Roughly half of the simulations in Table 4 utilize single-site (Lennard−Jones) representations of the solute and solvent. The remainder, many from our own work, incorporate more realistic, multisite solute/solvent models. The numbers in parentheses next to the species designations in Table 4 indicate the number of interaction sites employed in each case.

The experimental results in Table 5 include many data from our recent work on anthracene chromophores,[22] as well as a variety of other solutes whose characteristics vary over wide ranges. The supercritical solvents included in this collection are primarily those having critical points near to room temperature, because such solvents have been the most studied to date. An

TABLE 4: Summary of Augmentation Data and Potential Characteristics for Simulation Systems[a]

	solute	solvent	ref	#ρ	T/K	T/T_c	$\Delta\rho_{max}/\rho_c$	$(\rho_{eff}/\rho)_0$	V_{u0}	V_{uv}	$-B_{uv}$	K_{uv}	U_{uv}/ρ_v	α_{uv}	ϵ_{uv}	N_1^{est}
1	Ne(1)	Ne(1)	19	9	45	1.02	0.06_5	1.2_1	11	92	0.07	0.12	0.059	0.28	0.28	10
2	Xe(1)	Ne(1)	19	12	45	1.02	0.60_{10}	2.5_2	32	161	0.65	1.38	0.56	0.72	0.72	15
3	"DTBN"(1)	ethane(1)	27	10	330	1.08	0.37_{10}	2.8_4	393	1530	1.55	3.15	9.2	2.42	2.42	19
4	LJ(1)	CO_2(1)	30	6	310	1.02	0.31_7	1.9_3	26	211	0.40	0.86	2.2	3.27	3.27	10
5	anthracene(1)	CO_2(1)	30	6	310	1.02	0.41_7	2.0_3	165	605	1.16	2.46	6.2	3.27	3.27	20
6	pyrene(1)	CO_2(1)	26	8	308	1.02	0.42_{10}	2.1_3	191	684	1.28	2.72	6.9	3.21	3.21	20
7	"cufod"(1)	CO_2(1)	28	21	254	1.01	0.76_{10}	3.2_5	951	2400	6.84	14.6	36.7	3.37	3.37	34
8	cyclohexane(18)	CO_2(1)	31	10	323	1.06	0.26_5	1.9_3	106	436	0.59	1.43	3.8	3.72	3.81	17
9	benzene(12)	Ar(1)	29	9	168	1.04	0.43_{15}	2.5_{10}	112	410	0.89	1.03	3.3	2.44	2.71	19
10	anthracene(24)	CO_2(1)	30	19	310	1.02	0.41_{10}	2.2_4	204	714	1.11	1.58	8.0	4.12	4.78	22
11	anthracene(24)	CO_2(3)	30	6	310	1.02	0.25_{20}	1.8_5	204	778	1.05	1.43	9.6	3.97	7.15	21
12	anthracene+(24)	CO_2(1)	32	6	310	1.02	0.55_{15}	2.7_3	204	714	2.65	5.50	23.1	6.21	7.73	22
13	"C153"/S0(36)	Ethane(1)	33	10	310	1.02	0.78_{15}	3.7_5	249	1000	5.52	12.3	57.4	7.19	9.16	20
14	"C153"/S0(36)	CO_2(3)	33	11	310	1.02	0.63_{15}	3.9_5	249	948	3.33	7.41	36.2	5.93	10.11	22
15	"C153"/S1(36)	CO_2(3)	33	11	310	1.02	0.66_{15}	3.9_5	249	948	3.80	8.34	42.9	6.10	10.85	22
16	"C153"/q = 0(36)	CO_2(3)	33	2	310	1.02	0.43_{20}		249	948	2.56	5.82	24.5	5.17	8.04	22
									V_{v0}	V_{vv}	$-B_{vv}$	K_{vv}	U_{uv}/ρ_v	α_{vv}	ϵ_{vv}	N_1^{est}
		Ne(1)	19						11	92	0.07	0.12	0.35	0.28	0.28	10
		Ar(1)	29						21	165	0.11	0.19	0.37	1.01	1.01	10
		CO_2(1)	31						26	211	0.19	0.37	1.09	2.14	2.14	10
		CO_2(1)	26						29	229	0.16	0.28	0.97	1.87	1.87	10
		CO_2(1)	28						45	361	0.19	0.38	1.23	1.60	1.60	10
		CO_2(3)	30						28	240	0.17	0.26	1.20	1.65	3.16	10
		ethane(1)	33						40	324	0.30	0.59	1.68	2.15	2.15	10
		ethane(1)	27						74	596	0.27	0.56	2.00	1.61	1.61	10

[a] The data sources are indicated in the column "ref #". "#ρ" is the number of density points simulated. N_1^{est} is the estimated number of molecules in the first solvation shell of the solute (eq 19). Units of V_{i0} and V_{ij} are Å^3, B_{ij} and K_{ij} are in 10^3Å^3, α_{ij} and ϵ_{ij} are in kJ/mol; and U_{ij}/ρ_j in kJ·dm^3/mol.

important criterion used in selecting these data is proximity to the critical point, because this variable might be a primary factor governing the extent of density augmentation. The data collected here are therefore restricted to a range of reduced temperatures $1.01 \leq T/T_c \leq 1.08$, with the majority of the data lying between $T/T_c = 1.02 \pm .01$.

The two measures of local densities provided in Tables 4 and 5 are the maximum augmentation, $\Delta\rho_{max}$, and the enhancement factor extrapolated to zero density, $(\rho_{eff}/\rho)_0$. Examples of simulated and experimental data sets are provided in Figure 4, where we have also indicated the values assigned to these measures according to the methods outlined in Section II. The uncertainties shown in Figure 4 and listed in the tables reflect subjective estimates of the accuracy with which $\Delta\rho_{max}$ and $(\rho_{eff}/\rho)_0$ could be determined from the available data. As illustrated in Figure 4, the $\Delta\rho_{eff}(\rho)$ data are typically well-described by eq 2, so $\Delta\rho_{max}$ could be determined with reasonable certainty. The density at which $\Delta\rho_{eff}(\rho)$ is maximal was found to be fairly consistent among the various data sets, averaging $(0.68 \pm 0.11)\rho_c$ and $(0.61 \pm 0.11)\rho_c$ in the simulated and experimental systems, respectively. The density dependence of (ρ_{eff}/ρ) is more variable, and relatively large uncertainties are assigned to the $(\rho_{eff}/\rho)_0$ values for two reasons. First, in many systems, especially in experiments where solubility is limiting, data is not available at low densities ($\rho/\rho_c < 0.3$), so extrapolation to zero density is difficult. Second, the expected behavior of (ρ_{eff}/ρ) as $\rho \rightarrow 0$ is not always clear. In the majority of the collected data, (ρ_{eff}/ρ) appears to decrease with increasing density in the manner described by eq 3 and represented by the 9-cyanoanthracene data in Figure 4. However, simulations[19,26,28] and integral equation theories[20] on Lennard−Jones systems indicate that (ρ_{eff}/ρ) may reach a maximum at low but nonzero densities. The "cufod" data in Figure 4 provide an example of this type of behavior.[69] In the case of experimental data, it is often not clear whether such a maximum in ρ_{eff}/ρ is real or is due merely to large uncertainties in the data near the solubility limit. In the present work we ignore the distinction and simply utilize either the value extrapolated to $\rho = 0$ using fits to eq 3, or the value of (ρ_{eff}/ρ) estimated for some nonzero-density maximum, as the "limiting" value "$(\rho_{eff}/\rho)_0$". In doing so we accept rather large uncertainties in this measure of augmentation.

The effective densities reported in Table 4 (simulation data) all are defined in terms of the numbers of solvent atoms or molecules contained within the first solvation shell, as discussed in Section II.[70] Such data provide direct measures of local densities. In the case of the experimental data in Table 5, a variety of secondary observables ("Obs") have been used to determine local densities. The most plentiful data are from measurements of frequency shifts of electronic absorption or emission bands with density. The 9-cyanoanthracene data in Figure 4 derives from this type of experiment, and the analysis of such data is discussed in Section II (and in more detail in ref 22). Other observables, for example the rates associated with vibrational friction and relaxation,[39,40,42,71] have also been reported and can be used to characterize local densities. In all cases, if the original authors reported local densities, we adopt their values, possibly adjusting the data to conform to our choice of reference density. In cases where local densities were not reported, we reference the data to the density dependence expected for the observable in the absence of density augmentation. As an illustration, consider use of the Raman spectral data on the cyclopentane/CO_2 system reported by Pan and MacPhail.[39] These authors interpreted the spectral broadening observed in the C−H stretching spectrum of the cyclopentane solute in terms of the solvent-induced friction on its pseudorotation coordinate. The density dependence expected in the absence of solvent density inhomogeneities was described by these authors using an Enskog collision model. As a measure of density augmentation, we therefore used the departure of the observed values from the values predicted by this theoretical model. Of course, the effective densities so derived are only as reliable as the theoretical model with which one calibrates the "normal" density dependence. In addition to the uncertainties provided in Table 5, all of the experimental results incorporate further uncertainties

TABLE 5: Summary of Augmentation Data and Potential Characteristics for Experimental Systems[a]

#	solute[b]	solvent	ref # [c]	obs[d]	T/K	T/T_c	$\Delta\rho_{eff}/\rho_c$	$(\rho_{eff}/\rho)_0$	V_{u0}	V_{uv}	$-B_{uv}$	K_{uv}	U_{uv}/ρ_v	α_{uv}	ϵ_{uv}	N_1^{est}
1	CO_2	ethane	35	vib ν	313	1.03	-0.3_1	0.25_{10}	28	293	0.18	0.35	1.2	1.98	2.05	9
2	water	CO_2	45	NMR δ	313	1.03	0.36_{10}	2.3_4	17	180	0.20	0.46	0.2	2.93	5.86	9
3	methanol	CO_2	45	NMR δ	313	1.03	0.36_{10}	2.4_4	33	247	0.31	0.61	0.3	3.14	7.84	11
4	ethanol	CO_2	45	NMR δ	313	1.03	0.54_{10}	3.1_5	53	318	0.32	0.72	0.3	2.72	5.16	12
5	CH_2Cl_2	CO_2	45	NMR δ	313	1.03	0.19_{10}	1.9_4	57	331	0.33	0.74	0.2	2.42	3.78	13
6	benzene	CO_2	45	NMR δ	313	1.03	0.33_{10}	2.5_4	81	421	0.50	0.84	0.4	3.03	4.71	14
6	benzene	CO_2	41	abs ν	308	1.01	0.3_1	2.0_3	81	421	0.52	1.00	3.9	3.06	4.77	14
7	cyclopentane	CO_2	39	pr frict	323	1.06	0.3_2	1.4_5	84	431	0.35	0.85	2.6	2.22	3.66	15
8	chlorobenzene	CO_2	41	abs ν	308	1.01	0.79_{15}	3.2_5	92	470	0.63	1.22	4.6	3.10	4.83	15
9	cyclohexane	CO_2	42,39	vib Dp	323	1.06	0.15_8	1.8_2	99	477	0.42	1.04	3.0	2.37	3.87	15
10	2-nitroanisole	CO_2	34	abs ν	308	1.01	0.7_2	4.6_{15}	121	579	1.23	2.54	11.0	4.03	8.98	17
11	naphthalene	CO_2	41	abs ν	308	1.01	0.68_{10}	6.0_{15}	122	563	0.94	1.91	7.7	3.91	6.20	17
12	azulene	propane	40	abs ν	372	1.01	0.7_3	2.3_7	123	763	1.13	2.69	9.8	4.05	5.07	13
12	azulene	propane	40	vib rate	372	1.01	0.6_3	2_6	123	763	1.13	2.69	9.8	4.05	5.07	13
13	$W(CO)_6$	CO_2	44	vib ν	306	1.01	0.54_{15}	2.8_3	154	712	1.73	4.04	13.9	4.41	6.91	18
13	$W(CO)_6$	CHF_3	44	vib ν	301	1.01	0.60_{15}	2.8_5	154	817	2.32	5.30	2.0	5.23	7.31	16
13	$W(CO)_6$	ethane	44	vib ν	307	1.01	0.52_{15}	2.8_3	154	819	2.30	5.27	18.1	5.24	6.72	16
14	DTBN	ethane	23	ESR An	308	1.02	1.0_3	3.9_7	156	749	1.15	2.91	8.0	3.93	4.76	16
15	pyrene	CO_2	21	I1/I3	313	1.03	0.6_2	3.3_{10}	180	740	1.58	3.34	14.3	4.60	7.41	20
15	pyrene	CO_2	38	I1/I3	318	1.05	0.7_2	3.3_{10}	180	740	1.51	2.97	13.7	4.56	7.33	20
15	pyrene	CHF_3	21	I1/I3	305	1.02	1.0_2	4.3_{10}	180	846	3.28	7.28	39.2	6.54	11.5	17
16	anthracene	CO_2	22	em ν	308	1.01	0.79_{10}	3.4_8	162	708	1.43	2.65	12.5	4.39	7.20	19
16	anthracene	methanol	43	abs ν	523	1.02	0.44_{10}	2.2_5	162	707	0.56	1.16	7.8	4.22	6.17	18
16	anthracene	CHF_3	22	em ν	306	1.02	0.91_8	4.3_{10}	162	810	2.80	5.86	32.6	6.08	10.6	16
16	anthracene	ethane	22	em ν	311	1.02	0.90_{10}	3.9_{10}	162	810	1.77	3.67	13.7	4.36	5.45	16
17	9-CNAnth	CO_2	22	em ν	308	1.01	1.0_2	5.0_{15}	182	765	1.80	3.87	15.8	4.75	7.43	20
17	9-CNAnth	ethane	22	em ν	310	1.02	0.93_{10}	5.0_{10}	182	872	2.29	5.09	19.0	4.94	6.62	17
18	diClAnth	CO_2	22	em ν	308	1.01	0.83_{10}	4.5_{15}	185	777	1.74	3.63	15.2	4.71	7.63	20
18	diClAnth	CHF_3	22	em ν	304	1.02	0.90_{15}	4.8_{15}	185	887	2.83	6.24	29.3	5.96	9.49	17
18	diClAnth	ethane	22	em ν	310	1.02	0.91_{15}	5.7_{10}	185	886	2.43	5.44	20.7	5.14	7.00	17
19	diPhAnth	CO_2	22	em ν	308	1.01	0.94_{10}	5_2	303	1161	2.74	5.61	27.5	5.22	8.50	24
19	diPhAnth	CHF_3	22	em ν	304	1.02	1.03_{10}	5.3_{10}	303	1315	6.34	13.2	94.7	7.64	14.8	21
19	diPhAnth	ethane	22	em ν	310	1.02	0.88_8	4.4_{15}	303	1313	3.77	7.95	36.1	5.67	8.04	21
20	C153 (S0)	CO_2	24	exc ν	309	1.02	0.7_2	5.0_{15}	237	951	2.61	5.82	26.8	5.24	9.57	22
20	C153 (S1)	CO_2	24	em ν	309	1.02	0.9_2	6.8_{15}	237	951	3.07	6.73	33.3	5.53	10.5	22
20	C153 (S0)	ethane	24	exc ν	312	1.02	0.9_2	5.5_{15}	237	1082	3.19	7.18	31.0	5.70	7.99	19
20	C153 (S1)	ethane	24	em ν	312	1.02	0.9_2	4.8_{15}	237	1082	3.19	7.18	31.0	5.70	7.99	19
21	acetone	water	37	abs ν	663	1.02	0.52_{15}	2.8_8	63	282	0.11	0.22	3.2	4.78	9.75	16
22	benzophenone	water	37	abs ν	653	1.01	0.45_{10}	3.1_5	166	573	0.12	0.24	4.2	3.51	7.15	24
23	DEAEB (S1)	CHF_3	21	CT em ν	308	1.03	1.3_2	8_2	143	763	24.0	49.1	552	13.0	21.9	15
24	DMAEB (S0)	CHF_3	36	LE abs ν	303	1.01	1.0_2	6.1_{10}	143	749	2.73	6.76	30.0	6.32	11.0	15
25	DMABN (S0)	CHF_3	36	LE abs ν	301	1.01	1.0_2	5.2_{10}	143	749	2.79	6.89	30.8	6.35	11.0	15
17	9-CNAnth	CHF_3	22	em ν	306	1.01	0.87_8	5.5_8	182	847	3.59	7.92	40.9	6.55	10.9	17
20	C153 (S0)	CHF_3	24	exc ν	304	1.02	0.7_2	5.5_{15}	237	1082	9.29	20.5	169	9.77	18.5	19
20	C153 (S1)	CHF_3	24	em ν	304	1.02	0.9_2	6.9_{15}	237	1082	26.73	58.0	620	12.4	22.9	19
									V_{v0}	V_{vv}	$-B_{vv}$	K_{vv}	U_{uv}/ρ_v	α_{uv}	ϵ_{uv}	N_1^{est}
s1	CO_2	CO_2							28	240	0.16	0.32	1.2	1.65	3.14	10
s2	ethane	ethane							48	349	0.26	0.61	1.7	2.20	2.24	11
s3	propane	propane							66	493	0.37	0.83	3.0	2.59	3.24	10
s4	CHF_3	CHF_3							43	347	0.32	0.75	2.4	2.36	5.37	10
s5	methanol	methanol							33	254	0.31	0.60	5.9	5.52	24.3	10
s6	water	water							17	133	0.25	0.55	5.7	7.42	21.3	10

[a] N_1^{est} is the estimated number of molecules in the first solvation shell of the solute (see eq 19). Units of V_{i0} and V_{ij} are Å^3; B_{ij} and K_{ij} are in 10^3Å^3; α_{ij} and ϵ_{ij} are in kJ/mol, and U_{ij}/ρ_j are in in kJ·dm^3/mol. [b] Abbreviations are DTNB = di-*tert*-butylnitroxide, 9-CNAnth = 9-cyanoanthracene, diClAnth = 9,10-dichloroanthracene, di-PhAnth = 9,10-diphenylanthracene, C153 = coumarin-153, DEAEB = 4-*N*,*N*-diethylaminoethylbenzoate, DMAEB = 4-(*N*,*N*-dimethylamino)ethylbenzoate, DMABN = 4-(*N*,*N*-dimethylamino)benzonitrile. S0 and S1 denote the ground and first excited singlet electronic states. [c] Reference numbers to the original data sources. [d] Observable properties used to measure local densities: "NMR δ" denotes a ^{1}H chemical shift; "em ν", "abs ν", and "exc ν" denote frequencies of electronic emission, absorption, and excitation spectra; "vib ν" denotes vibrational frequencies; "vib dp" and "vib rate" denote the rate of vibrational phase and population relaxation, respectively; "ESR An" denotes a hyperfine splitting constant; "I1/I3" denotes an emission peak intensity ratio; and "CT" and "LE" denote charge-transfer and locally excited electronic states. See original references for details.

due to possible errors in the assumptions needed to connect the experimental observable to density.

V. Solute−Solvent Interactions and Density Augmentation

Table 6 lists the characteristics to be correlated to the augmentation data. Most gauge the interactions between the solute and solvent in the limit of zero density. In addition to the six solute−solvent ("uv") characteristics already catalogued in Table 1, a variety of other, composite characteristics are considered. The latter quantities involve mainly thermal ratios or ratios of solute−solvent to solvent−solvent properties possibly relevant to the augmentation problem. For example, examination of the pair energy density and the relative energy density are motivated by the theoretical analysis of van der Waals fluids by Petsche and Debenedetti.[11] We also compute three further quantities meant to approximate features of

TABLE 6: Correlations between Intermolecular Potential Characteristics and Measures of Density Augmentation[a]

		simulation		experiment		
characteristic	interpretation	f_Δ	R	f_Δ	R	R(np)
V_{u0}	solute volume	4	0.43	1	0.28	0.17
V_{uv}	uv excluded volume	3	0.47	2	0.67	0.72
B_{uv}	uv virial coefficient	3	0.81	9	0.56	0.68
K_{uv}	uv association constant	3	0.81	8	0.57	0.68
(U_{uv}/ρ_v)	solvation energy per solvent molecule	4	0.78	10	0.48	0.58
α_{uv}	uv free energy parameter	2	0.59	2	0.74	0.76
ϵ_{uv}	uv potential energy parameter	2	0.58	2	0.68	0.68
V_1^{est}	first solvation shell volume (eq 3−1)	2	0.41	1	0.65	0.66
N_1^{est}	coordination # at $2\rho_c$ (est; eq 3−2)	1	0.54	1	0.51	0.70
$\Delta G_{uv}/k_BT$	free energy of association	0.6	0.83	0.7	0.78	0.80
U_{solv}^{est}/k_BT	solvation energy at $2\rho_c$ (est; eq 3−3)	3	0.85	10	0.49	0.61
α_{uv}/k_BT	free-energy Boltzmann factor	1	0.76	2	0.75	0.77
ϵ_{uv}/k_BT	potential-energy Boltzmann factor	2	0.66	3	0.71	0.69
V_{u0}/V_{v0}	relative size	3	0.48	2	0.41	0.61
$(\Delta G_{uv} - \Delta G_{vv})/k_BT$	relative association free energy	2	0.88	3	0.76	0.82
U_{uv}/U_{vv}	relative solvation energy	3	0.80	10	0.51	0.68
α_{uv}/α_{vu}	relative free energy parameter	1	0.80	2	0.74	0.76
$\epsilon_{uv}/\epsilon_{vv}$	relative potential energy parameter	1	0.79	2	0.68	0.68
ϵ_{uv}/V_1^{est}	pair energy density	2	0.35	2	0.26	0.14
$(\epsilon_{uu}/V_{u0})/(\epsilon_{vv}/V_{v0})$	relative energy density	2	0.37	4	0.14	−0.08

[a] The R values here are the average of the linear correlation coefficients between the two density measures $\Delta\rho_{max}$ and $(\rho_{eff}/\rho)_0$ and the potential characteristics listed. The correlations include all of the data listed in Table 4 and all of the unique solute/solvent combinations listed in Table 5 (38 points). In cases where more than one experimental measurement was available on a given solute−solvent pair, average values were used in the regressions. The final column "R(*np*)" lists the experimental correlations observed when the "polar" systems (solute #21 and lower in Table 3) are excluded from the analysis (32 points included). The columns labeled f_Δ denote the variability of the various characteristics over the data sets as defined by eq 21.

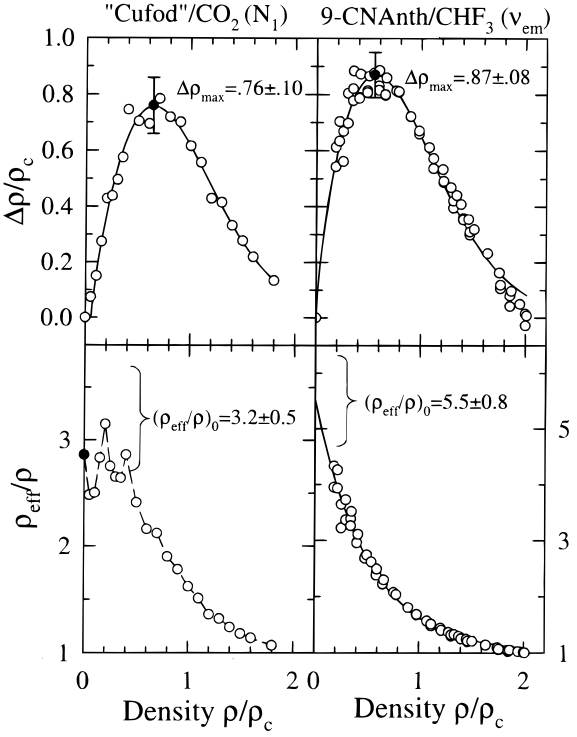

Figure 4. Representative augmentation data illustrating the assignment of values of $\Delta\rho_{max}$ and $(\rho_{eff}/\rho)_0$ and their uncertainties. The left-hand panels are data from the Lennard−Jones simulations of "cufod" in CO_2 by deGrazia et al.,[28,69] and the right-hand panels show data on 9-cyanoanthracene in CHF_3 from ref 22.

solvation expected in the dense solvent limit (i.e., at ρ_{ref}). The volume of the first solvation shell of the solute is approximated by

$$V_1^{est} \equiv \{V_{u0}^{1/3} + V_{vv}^{1/3}\}^3 - V_{u0} \qquad (18)$$

On the basis of this volume, the coordination number (the number of solvent molecules expected in the first solvation shell of the solute) at the reference density $2\rho_c$ is estimated using the relation

$$N_1^{est} \equiv 3.16(V_1^{est}/V_{vv}) \qquad (19)$$

The numerical factor of 3.16 in this expression derives from simulation results available at high density. For the 15 simulations for which coordination numbers were available or could be estimated,[72] the observed values of N_1 agree with those estimated using eq 19 to within a standard deviation of 10%. Finally, the solvation energy, or solute−solvent potential energy at the reference density, was estimated using the relation

$$U_{solv}^{est} \equiv 0.66(U_{uv}/\rho_v)\rho_c \qquad (20)$$

The numerical factor 0.66 again comes from a calibration using solvation energies measured in simulation. These estimated solvation energies are less accurate than the coordination numbers, with the standard deviation of the ratio $U_{solv}^{est}/U_{solv}^{obs}$ being as large as 40%. Nevertheless, eq 20 provides at least a first estimate of relative solvation energies expected in the dense solvent limit.

Before discussing how the calculated quantities relate to density augmentation, we should recognize that the various characteristics listed in Table 6 are far from independent. Some relationships among the primary quantities (i.e., those in Table 1) are shown in Figure 5. The top two panels of Figure 5 display the correlations present in the set of properties $\{B_{uv}, K_{uv}, (U_{uv}/\rho_v)\}$, all of which derive from integrals over various Boltzmann factors (eqs 7, 10, and 12). The top panel of Figure 5 shows that a high degree of correlation exists between the magnitude of the second-pressure virial coefficient B_{uv} and the association constant K_{uv} of a given $u-v$ pair. A quantitative measure of this correlation is provided by the linear correlation coefficient[73] "R". The value $R = 0.99$ for this logarithmic plot indicates that

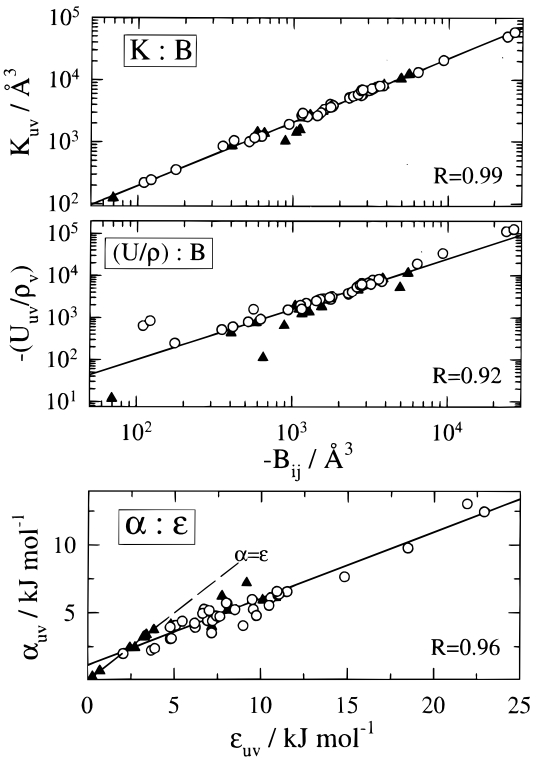

Figure 5. Illustration of the correlations observed between various calculated properties. Solid triangles denote data from simulation systems; open circles represent those from experimental systems. Solid lines and the correlation coefficients (R) listed in the figure refer to regressions including the combined set of independent simulation and experimental data (50 systems).

a nearly exact linear relationship exists between ln B_{uv} and ln K_{uv} (perfect correlation being defined by $R = \pm 1$). What this near-perfect correlation means is that B_{uv} and K_{uv} provide essentially equivalent measures of some aspect of the $u-v$ interaction. The "solvation energy" integral (U_{uv}/ρ_v) and B_{uv} (middle panel of Figure 5), as well as K_{uv} and (U_{uv}/ρ_v), are also strongly correlated, albeit to a lesser extent than B_{uv} and K_{uv}. Thus, the three parameters B_{uv}, K_{uv}, and (U_{uv}/ρ_v) are largely redundant in their information content. In contrast, the simple volume integrals $\{V_{uv}, V_{u0}\}$, provide substantially independent information ($R \sim 0.3$ with the former quantities). Intermediate between these extremes, we find moderate overlap between the set $\{B_{uv}, K_{uv}, (U_{uv}/\rho_v)\}$ and the energy parameters α_{uv} and ϵ_{uv}. The linear correlation coefficients across the two sets are in the range 0.80−0.85. The two effective well depths α_{uv} and ϵ_{uv} are strongly correlated to one another, as illustrated in the bottom panel of Figure 5. Such a correlation is not surprising given the fact that for spherically symmetric $u-v$ interactions, these two energies are necessarily equal. (The filled triangles falling along the $\alpha = \epsilon$ line in Figure 5 are the single-site solute−solvent representations used in some of the simulations, which adhere to this equality.) In the absence of such symmetry, the free-energy well (measured by α) is always shallower than the potential energy well (ϵ), and on average we find $\alpha/\epsilon = 0.6 \pm 0.1(1\sigma)$ for the collection of experimental systems studied here. Finally, it should also be noted that the composite characteristics derived from these primary quantities will often be substantially correlated with them, by virtue of the nature of the data sets employed. For example, α_{uv}/k_BT is far from independent of α_{uv} ($R = 0.93$) because of the small range of temperatures spanned by the majority of the data. Likewise, ratios such as α_{uv}/α_{vv} are correlated to α_{uv}/k_BT ($R = 0.92$) by virtue of the fact that all

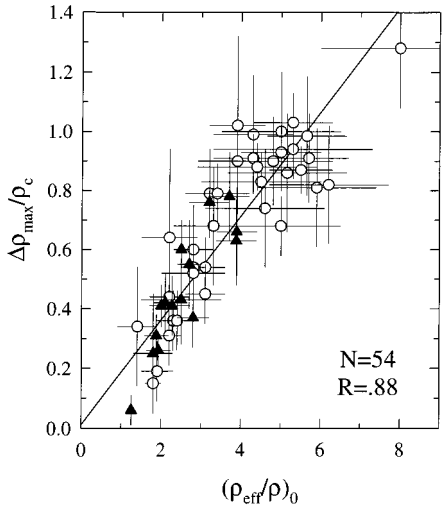

Figure 6. Comparison of the two measures of density augmentation $\Delta\rho_{max}$ and $(\rho_{eff}/\rho)_0$. Filled triangles are data from simulation and open circles are from experiment.

observations are taken near the critical temperature of the solvent, and this temperature is in turn dictated by a solvent−solvent energy parameter such as α_{vv}. The conclusion to be drawn from this discussion is that the "different" quantities characterizing intermolecular interactions in Table 6 form a highly interdependent set.

It is also useful to note that a clear correlation exists between the two measures of density augmentation, $\Delta\rho_{max}$ and $(\rho_{eff}/\rho)_0$. Figure 6 illustrates the relationship for both the simulation (filled triangles) and experimental (open circles) data sets. The presence of such a correlation, although not surprising, is not necessary. If the $(\rho_{eff}/\rho)_0$ data truly reflect the $\rho = 0$ limit, they should contain information distinct from $\Delta\rho_{max}$ for the reason that only pairwise solute−solvent interactions are relevant at $\rho = 0$, whereas the densities at which $\Delta\rho$ is maximal are far from this isolated pair limit. (In fact, if the $(\rho_{eff}/\rho)_0$ data are really $\rho = 0$ results they should be interpretable solely on the basis of pair calculations of the sort performed here.[74]) The fact that we do observe a good correlation between $(\rho_{eff}/\rho)_0$ and $\Delta\rho_{max}$ might merely reflect the fact that extrapolating data from higher densities (mostly far from $\rho = 0$) does not provide the zero-density behavior, but is reflective of the same density regime as $\Delta\rho_{max}$. Alternatively, the values of $(\rho_{eff}/\rho)_0$ determined here could indeed reflect the low-density limit, in which case the correlation with $\Delta\rho_{max}$ would indicate that binary interactions largely dictate the density augmentation observed at near-critical densities. Although the latter interpretation is consistent with the underlying premise of the present study, the data provide no clear indication of which interpretation is correct. In light of the high degree of correlation between these two measures of density augmentation, in Table 6 we have averaged the results obtained in separate correlations to $\Delta\rho_{max}$ and $(\rho_{eff}/\rho)_0$ in order to simplify the presentation.

Now, consider the correlations between density augmentation and the various potential-derived properties. The main results are provided in the form of linear correlation coefficients for the simulated and experimental data sets in Table 6. Some of the best correlations found are also shown graphically in Figures 7 and 8. Also listed in Table 6 are the "fractional variations",

$$f_\Delta(X) \equiv \frac{\max(X) - \min(X)}{\text{average}(X)} \qquad (21)$$

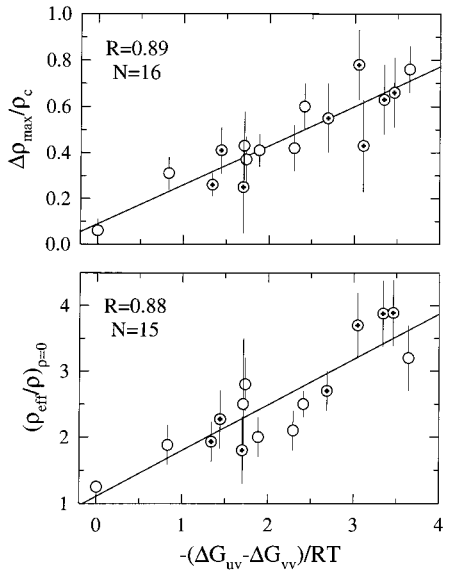

Figure 7. Plots of $\Delta\rho_{max}$ and $(\rho_{eff}/\rho)_0$ versus the relative free energy of association $(\Delta G_{uv} - \Delta G_{vv})/k_BT$ for the simulated data in Table 4. The "+" signs within some symbols designate multisite solute and/or solvent representations.

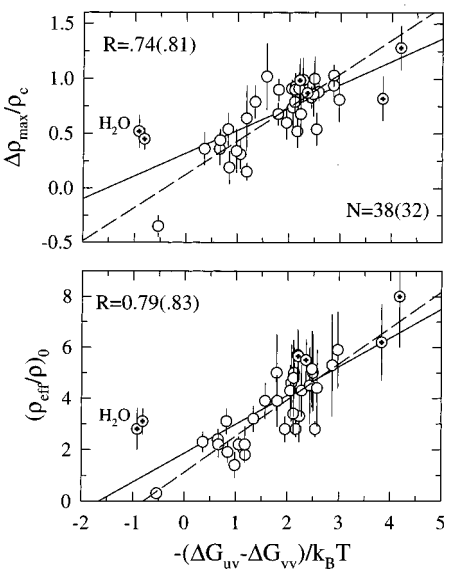

Figure 8. Plots of $\Delta\rho_{max}$ and $(\rho_{eff}/\rho)_0$ versus the relative free energy of association $(\Delta G_{uv} - \Delta G_{vv})/k_BT$ for the experimental data in Table 5. Solid lines are linear fits to all 38 distinct solute/solvent pairs, which yield the correlation coefficients indicated. The "+" signs within some symbols designate polar−polar solute−solvent combinations, for which the uncertainties in the potential-derived quantities are likely to be largest. The dashed lines are the fits to the 32 points excluding these polar data. Regression coefficients are shown in parentheses. "H_2O" labels data for the benzophenone−water and acetone−water systems, as discussed in the text.

which are intended to measure the variability of each property over the available data.

Consider first the comparisons to simulated augmentation data. As a guide to interpreting the R values listed in Table 6, we note that in a sampling of 14 independent[75] (x_i, y_i) pairs, there is a 5% probability of measuring a value of $R \geq 0.53$ if the two observables x_i and y_i are truly independent. Thus, one can say with 95% confidence that values of R larger than 0.53 reflect some genuine link between density augmentation and the property considered. Table 6 shows that only the simple volumetric properties (V_{uv}, V_1^{est}, V_{uv}/V_{vv}) and the energy densities involving them lie below this cutoff. For the remaining properties, R is greater than 0.53, and in nine cases a high degree of correlation ($R \geq 0.8$) with density augmentation is found. Among the primary set, the integral quantities B_{uv}, K_{uv}, and (U_{uv}/ρ_v) all show a high level of correlation, whereas the well depths α_{uv} and ϵ_{uv} do not. Much better correlations involving the latter quantities occur for the ratios α_{uv}/α_{vv} and $\epsilon_{uv}/\epsilon_{vv}$. Finally, the best correlators of the extent of density augmentation appear to be the association free energies $\Delta G_{uv}/k_BT$ and $(\Delta G_{uv} - \Delta G_{vv})/k_BT$.

The correlation between the simulated values of augmentation and the free-energy difference $(\Delta G_{uv} - \Delta G_{vv})/k_BT$ is illustrated in Figure 7. The points containing "+" symbols in this figure denote polyatomic solute and/or solvent representations, whereas the remainder are data from simulations of Lennard−Jones models. No distinction is found between these two types of model systems, either in Figure 7 or in similar comparisons with other properties examined. This consistency is noteworthy in that it helps validate the widespread practice of modeling supercritical systems with idealized Lennard−Jones representations. Also shown in Figure 7 are the least-squares fits to linear relationships between $(\Delta G_{uv} - \Delta G_{vv})/k_BT$ and the augmentation measures. There is no particular justification for assuming that $\Delta\rho_{max}$ or $(\rho_{eff}/\rho)_0$ should be *linearly* related to $(\Delta G_{uv} - \Delta G_{vv})/k_BT$, but such a relationship is not unreasonable. In fact, if one interprets the uncertainty estimates listed in Table 4 (plotted as error bars in Figure 7) as standard deviations, one finds the goodness-of-fit statistics[73] χ_ν^2 to be 0.56 and 1.08, respectively, for these linear fits. The probabilities (P) of observing values of χ_ν^2 at least this large in linearly related data with such uncertainties are 85% and 35%, respectively. Thus, to the extent that our estimates of uncertainty are reasonable, the present data do support a simple linear model. The situation is only slightly less favorable in the case of linear fits of $\Delta G_{uv}/k_BT$ to $\Delta\rho_{max}$ and $(\rho_{eff}/\rho)_0$, for which $\chi_\nu^2 = 1.09$ ($P = 35\%$) and 1.57 ($P = 10\%$). For the remaining potential-derived properties, such analysis shows a linear model to be inadequate. Nevertheless, the fact remains at there is a close relationship between these potential-derived quantities and density augmentation. Thus, the primary question posed by the present work—"is the extent of density augmentation simply related to some measure of the strength of intermolecular interactions?"—can be answered affirmatively, at least in the case of simulated data.

Next, consider these same correlations using experimental data. In doing so, one should keep in mind that the experimental comparisons incorporate two sources of uncertainty not present in the simulation case. First, whereas true local densities are measured in simulation, the effective densities determined experimentally are filtered through a variety of experimental observables whose relationship to density is not known with certainty. Second, the intermolecular potential functions, from which the calculated properties are derived, are known exactly in the simulation case, whereas in the case of experiment they are only reasonable approximations to the true potentials. Despite these extra uncertainties, Table 6 shows that the correlations found with the experimental data set (38 independent solute/solvent pairs[75]) are often comparable to those obtained with the simulated data. The only quantities for which the experimental correlation coefficients are much smaller than their simulation counterparts involve the quantities B_{uv}, K_{uv}, and U_{uv}. The difference in these cases is due to the greater variatiability (f_Δ) of these properties in the experimental data set. This greater variability is in turn due primarily to extreme values occurring in some polar solute/solvent pairs, which were

not studied by simulation. Because the results of the previous section suggest that the calculated quantities might contain substantial errors when polar interactions predominate, Table 6 includes a listing of the correlation coefficients obtained when only the 32 unique "nonpolar" solute−solvent pairs, pairs in which at least one member is nondipolar, are considered. Removing the polar systems makes the simulated and experimental data sets more similar, and also renders the correlation coefficients involving B_{uv}, K_{uv}, and U_{uv} closer to the simulation values. It also generally increases the remaining correlation coefficients, but the effect is relatively modest.[76] Either with or without the polar data, the results in Table 6 reveal definite relationships between the experimental density augmentation and the pair potential characteristics calculated here. For 38 independent points, the 95% confidence limit for correlation occurs at an R value of 0.34.[73] Again, only the simple volumetric and the energy density parameters lie below this breakpoint, meaning that all of the other calculated quantities are related, in some manner, to the extent of density augmentation. As with the simulated data, the highest correlation coefficients are again found for the association free energies $\Delta G_{uv}/k_BT$ and $(\Delta G_{uv} - \Delta G_{vv})/k_BT$, and for the free-energy parameters α_{uv}/k_BT and α_{uv}/α_{vv}.

Figure 8 displays the correlation between the experimental augmentation data and $(\Delta G_{uv} - \Delta G_{vv})/k_BT$. Embedded "+" symbols now indicate polar solute/solvent pairs, and the solid and dashed lines are the linear regressions to the full and the nonpolar data sets, respectively. The presence of a relationship between the calculated free-energy difference and the augmentation data is obvious from this figure, especially using the $(\rho_{eff}/\rho)_0$ measure of augmentation. We note that there are two points, labeled "H_2O" in Figure 8, which correspond to the solute−solvent pairs acetone−water and benzophenone−water, that deviate markedly from the trend established by the remaining data. Similar deviations are found in plots of the other free-energy parameters mentioned above. In fact, at least for these properties, removing these two data points yields correlation coefficients slightly better than those listed in Table 6 for the nonpolar data set. We therefore digress momentarily to consider the source of the deviation of these two systems.

The acetone−water and benzophenone−water systems are unique in that the UV absorption data indicate substantial density augmentation,[37] but the calculations indicate $\Delta G_{uv} > \Delta G_{vv}$, i.e., that solute−solvent association is less favorable than solvent−solvent association. The only other example of such a predicted energy ordering is for the first system listed in Table 3, the combination CO_2−ethane. In this latter case, vibrational frequency measurements[35] indicate that the density around the CO_2 solute is actually depleted rather than augmented ($\Delta\rho < 0$). This behavior would be anticipated if the solute−solvent interactions were less attractive than the solvent−solvent interactions.[1] The contrary and counterintuitive behavior of the acetone−water and benzophenone−water systems probably results from inaccuracies in the interaction potentials used here, which apparently predict the wrong sign for $(\Delta G_{uv} - \Delta G_{vv})$. Such an error might result from neglect of explicit polarizability in the potentials, as discussed in Section III, with respect to their poor performance in predicting virial coefficients involving water with nonpolar partners. On the basis of that discussion, we anticipate the strength of acetone−water and benzophenone−water pair interactions to be underestimated, and that of water−water interactions to be overestimated, by the potentials employed here. We note that a 35% increase in ΔG_{uv} ($\sim 2k_BT$) would be required to move these two water points into line with the remaining data. An error of this magnitude is consistent with the errors (for example, the γ values) observed in the virial predictions made for similar systems. We therefore omit these two data points from further analysis.

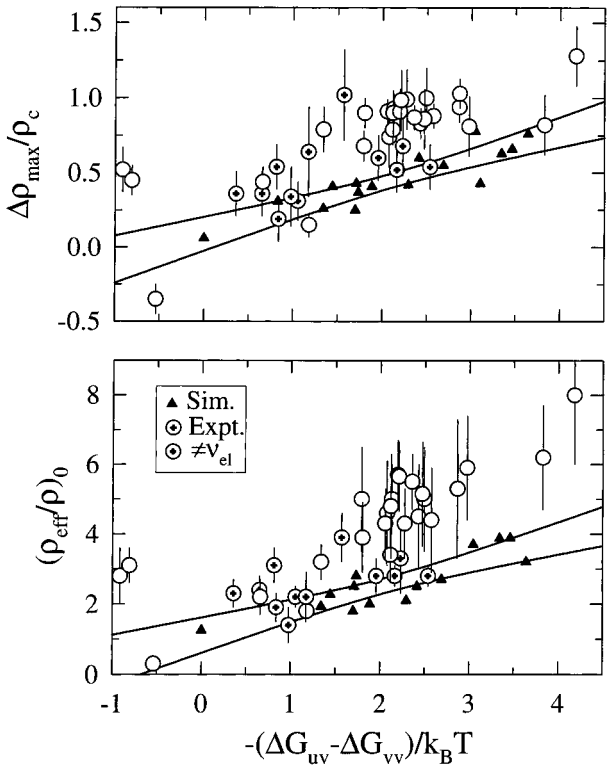

Figure 9. Comparison of the correlations found for the experimental (large open symbols) and simulation (filled triangles) data sets. The curved lines indicate the 95% confidence limits of the fit of the simulation data to a line. The "+" signs within some symbols designate experimental data that were not determined from measurements of the frequency shifts of electronic spectra.

Returning now to the overall correlations displayed in Figure 9, we can ask whether the remaining experimental data support the existence of a simple linear relationship between $\Delta\rho_{max}$ or $(\rho_{eff}/\rho)_0$ and $(\Delta G_{uv} - \Delta G_{vv})/k_BT$. Using estimated uncertainties to represent standard deviations, we find values of $\chi_\nu^2 \sim 2.0$ ($P < 1\%$) in both cases. (Approximately the same statistics are obtained if all polar pairs are excluded.) Thus, if the uncertainties are appropriate, the experimental data do not support a linear relationship between either measure of density augmentation and this or any of the other free-energy parameters. However, as in the case of the simulated data, all of the free-energy parameters $(\Delta G_{uv} - \Delta G_{vv})/k_BT$, $\Delta G_{uv}/k_BT$, α_{uv}/k_BT, and α_{uv}/α_{vv} nevertheless provide useful indicators of the observed density augmentation. Given the similar results for both the experimental and the simulated data sets, we therefore conclude that these free-energy quantities must encode the majority of the information needed to predict the extent of augmentation in a given system.

Finally, we consider the relationship between the experimental and the simulated augmentation data, which is displayed in Figure 9. The curved lines in this figure represent the 95% confidence limits of the linear fit to the simulated data (filled triangles), and the symbols with error bars are the experimental points. Although there is some overlap, the two data sets clearly do not follow the same correlation with $(\Delta G_{uv} - \Delta G_{vv})/k_BT$. The experimental data generally show greater augmentation than the corresponding simulation data for a given value of the

TABLE 7: Direct Simulation/Experiment Comparisons[a]

solute[b]	solvent	ϵ_{uv}/kJ mol^{-1}	$\Delta G_{uv}/k_BT$	$\Delta\Delta G/k_BT$	$\Delta\rho_{max}/\rho_c$[c]	$(\rho_{eff}/\rho)_0$[c]	ref #
cyclohexane(18)	CO_2	3.8/3.9	7.3/6.9	1.3/1.2	$.26_5/0.15_8$	$1.9_3/1.8_2$	31/42
DTBN(1)	ethane	2.4/4.8	8.1/8.0	1.7/1.6	$.37_{10}/1.0_3$	$2.8_4/3.9_7$	27/23
pyrene(1)	CO_2	3.2/7.3	7.9/8.0	2.3/2.2	$.42_{10}/0.7_2$	$2.1_3/3.3_{10}$	26/21&38
anthracene(24)	CO_2	6.0/7.2	7.3/7.9	1.6/2.1	$.33_{15}/0.79_{10}$	$2.0_5/3.4_8$	30/22
C153(36)	ethane	9.2/10.0	9.4/8.7	3.0/3.0	$.78_{15}/0.8_2$	$3.7_5/5.9_{15}$	33/24
C153(36)	CO_2	10.5/8.0	9.0/8.9	3.4/2.5	$.65_{15}/0.9_2$	$3.9_5/5.2_{15}$	33/24

[a] Paired data of the form "x/y" indicate the values from simulation (x) and experiment (y). [b] Values in parentheses indicate the number of interaction sites employed in the simulations. In all but the C153/CO_2 simulations, where CO_2 was represented by three sites, the simulated solvents were represented as single Lennard−Jones sites. [c] Subscripts indicate estimated uncertainties in the final digit(s).

correlating parameter $(\Delta G_{uv} - \Delta G_{vv})/k_BT$. This result is independent of the particular property chosen for correlation, as one might guess from the fact that a majority of the experimental augmentation values lie above all of the simulated values (see also Figure 6). Such a result could reflect the fact that the systems chosen for simulation differ on average from those studied in experiment, in some aspect not captured by the potential-derived properties considered here. However, we note that a number of simulations have been undertaken specifically for purposes of comparison to experimental systems. The results of such comparisons, collected in Table 7, exhibit the same dichotomy observed more generally in Figure 9. Thus, there appears to be a general disagreement between the extent of density augmentation determined in simulation and that measured in experiment.

VI. Summary and Conclusions

The purpose of the present study was to bring together available data on solvation in supercritical solvents and to use them to quantitatively examine the relationship between density augmentation and characteristics of the solute−solvent interaction potential. As a byproduct of this effort, we also provided some assessment of the accuracy of commonly used intermolecular potentials for predicting pair interaction properties. The main results of this study can be summarized as follows:

1. *Standard potential functions are reliable for calculating the binary interactions between most of the solute−solvent and solvent−solvent pairs of interest here.* In this study, interactions were modeled using the same sorts of pairwise additive effective potentials commonly employed in simulations of condensed phases. Potential models previously optimized to reproduce the liquid−vapor coexistence properties of the pure fluids were used to represent solvent molecules. For solutes, geometries and charges from electronic structure calculations were combined with standard Lennard−Jones parameters taken from the OPLS set.[59,60] The accuracy of these potentials was tested against experimental data on second-pressure virial coefficients for both like and unlike pairs. In the case of like interactions, such potentials were found to overestimate the strength of the interactions between nondipolar molecules by 4−10% and to underestimate them in the polar supercritical solvents examined by up to 20%. The direction and approximate magnitude of these errors are consistent with the known differences between true pair potentials and the effective potentials used for condensed-phase simulation. Similar results were also found for most unlike pair interactions. Overall, the types of potentials used here appear to be accurate to the level of ±10% for reproducing direct energy quantities and to ±20% for reproducing Boltzmann-weighted quantities such as virial coefficients of nonpolar or weakly polar pairs. Interactions involving highly polar pairs are predicted less accurately, but are still in reasonable accord with the experiment. The most notable failure of these potentials occurs in highly polar−nonpolar pairs such as water−Ar. In such pairs, neglect of explicit polarizability leads to interaction strengths that are too low by some 30−40% and to errors in derived pair properties that may be even larger.

2. *The density dependence of effective local densities is similar in a variety of experimental and simulated systems.* The data collected here comprise simulations of 14 distinct solute−solvent pairs and experimental results on 38 distinct pairs. Effective local densities were defined relative to a reference density of $2\rho_c$, where local and bulk densities are assumed to be identical. At other densities, the difference between local and bulk behavior was characterized by examining how both the "augmentation" $\Delta\rho_{eff} = \rho_{eff} - \rho$ and the "enhancement factor" ρ_{eff}/ρ vary with bulk density ρ. To within uncertainties, these two functions showed similar behavior in a variety of systems. The augmentation generally peaks at densities of $(0.65 \pm 0.11)\rho_c$, and the enhancement in most (but not all) systems is a monotonically decreasing function of density. From the density-dependent data, two quantities served to summarize the extent of density augmentation in a given system: the maximum augmentation $\Delta\rho_{max}$ and the enhancement factor at zero-density $(\rho_{eff}/\rho)_0$. In principle these two measures emphasize different density regions and might therefore be expected to contain distinct information. However, $\Delta\rho_{max}$ and $(\rho_{eff}/\rho)_0$ were found to be strongly correlated to one another in the systems examined.

3. *The extent of local density augmentation depends on the strength of solute−solvent interactions in the expected manner.* We calculated a variety of different, albeit inter-related, volumetric and energetic characteristics of the interactions between solute and solvent pairs and many were found to have significant correlations with $\Delta\rho_{max}$ and $(\rho_{eff}/\rho)_0$. The highest linear correlations were found for characteristics involving the free energies α_{uv}, the average free energy of the uv pair at contact (Figure 2), and ΔG_{uv}, the free energy of association (eq 11). Correlations to analogous potential energy quantities such as ϵ_{uv} and (U_{uv}/ρ_v) were of lesser quality. The best indicators of density augmentation observed in both the experimental and the simulated data sets were found to be the quantities $\Delta G_{uv}/k_BT$ and $(\Delta G_{uv} - \Delta G_{vv})/k_BT$. Both $\Delta\rho_{max}$ and $(\rho_{eff}/\rho)_0$ could be fitted to linear functions of either of these free-energy parameters nearly to within their (admittedly large) uncertainties. Although the correlations reported here are far from perfect, it is significant that a single quantity[77] such as ΔG_{uv}, which involves only the interaction between pairs of molecules, is capable of systematizing the augmentation observed in a diverse range of solute−solvent pairs. This observation indicates that although density augmentation may be tied to the complex collective behavior of fluids near their critical points, the primary determinant of the variations observed among different systems is the relative attraction between the solute and solvent. As noted in the Introduction, the similar local densities exhibited by many systems, most notably among the set of 12 substituted an-

thracene/solvent pairs recently examined,[22] appeared to contradict this intuitive notion. However, the present analysis suggests that the similar augmentation behavior of these systems mainly reflects the fact that the key quantities $\Delta G_{uv}/k_BT$ and especially $(\Delta G_{uv} - \Delta G_{vv})/k_BT$ vary relatively little among these solute/solvent combinations.

4. *A systematic difference is observed between simulated and experimental measurements of density augmentation*. Perhaps the most surprising result of the present work was observation that the extent of local density augmentation deduced from experimental measurements tends to be larger than that obtained by simulation. Two explanations of this difference seem reasonable. The first is that the simulations performed to date fail to capture the true extent of density augmentation found in real systems. Such a failure might arise from the difficulty in sampling the large/slow fluctuations present at near-critical temperatures.[78,79] Alternatively, there could be some underlying problem with experimental measurement of density augmentation. The most likely source of error is inaccuracies in how the quantities actually measured in the experiment are interpreted in terms of local densities. Most experimental studies of local density augmentation to date have measured shifts of electronic spectra. It is noteworthy that the few experimental points we have collected that are not based on electronic shifts (marked with "+" symbols in Figure 9) appear to be in better agreement with the simulation results than the remainder of the data. This observation suggests that it might be useful to reexamine the theoretical basis for relating electronic shifts to solvent density.

Acknowledgment. The authors thank Sergei Egorov for useful discussions concerning this work and for sharing the results of ref 20 prior to publication. This work was supported by a grant from the National Science Foundation (CHE-9980383).

Supporting Information Available: Tables showing potential parameters for simulated systems. This material is available free of charge via the Internet at http://pubs.acs.org.

References and Notes

(1) Debenedetti, P. G.; Mohamed, R. S. *J. Chem. Phys.* **1989**, *90*, 4528.
(2) Fernandez-Prini, R.; Japas, M. L. *Chem. Soc. Rev.* **1994**, 155.
(3) Noyori, R., Ed. *Chem. Rev.* **1999**, *99*, 353.
(4) References 2, 6, 13, and especially ref 5 provide recent reviews of much of the research on solvation and density augmentation in supercritical fluids.
(5) Tucker, S. C. *Chem. Rev.* **1999**, *99*, 391.
(6) Kajimoto, O. *Chem. Rev.* **1999**, *99*, 355.
(7) van Wasen, U.; Schneider, G. M. *J. Phys. Chem.* **1980**, *84*, 229.
(8) Eckert, C. A.; Ziger, D. H.; Johnston, K. P.; Ellison, T. K. *Fluid Phase Equilib.* **1983**, *14*, 167.
(9) Wheeler, J. C. *Ber. Bunsen.-Ges. Phys. Chem.* **1972**, *76*, 308.
(10) Eckert, C. A.; Ziger, D. H.; Johnston, K. P.; Kim, S. *J. Phys. Chem.* **1986**, *90*, 2738.
(11) Petsche, I. B.; Debenedetti, P. G. *J. Phys. Chem.* **1991**, *95*, 386.
(12) Chialvo, A. A.; Cummings, P. T. *AIChE J.* **1994**, *40*, 1558.
(13) Tucker, S. C.; Maddox, M. W. *J. Phys. Chem. B* **1998**, *102*, 2437.
(14) Maddox, M.; Goodyear, G.; Tucker, S. *J. Chem. Phys.* **2000**, in press.
(15) Kajimoto, O.; Futakami, M.; Kobayashi, T.; Yamasaki, K. *J. Phys. Chem.* **1988**, *92*, 1347.
(16) Morita, A.; Kajimoto, O. *J. Phys. Chem.* **1990**, *94*, 6420.
(17) Subramanian, R.; Pyada, H.; Lira, C. *Ind. Eng. Chem. Res.* **1995**, *34*, 3830.
(18) Petsche, I. B.; Debenedetti, P. G. *J. Chem. Phys.* **1989**, *91*, 7075.
(19) Egorov, S. A.; Yethiraj, A.; Skinner, J. L. *Chem. Phys. Lett.* **2000**, *317*, 558.
(20) Egorov, S. A. *J. Chem. Phys.* **2000**, *112*, 7138.
(21) Sun, Y. P.; Bunker, C. E. *Ber. Bunsen-Ges. Phys. Chem.* **1995**, *99*, 976.
(22) Lewis, J.; Biswas, R.; Robinson, A.; Maroncelli, M. The Solute and Solvent Dependence of Local Density Augmentation in Supercritical Fluids. *J. Phys. Chem. A*, to be submitted for publication.
(23) Carlier, C.; Randolph, T. W. *AIChE J.* **1993**, *39*, 876.
(24) Biswas, R.; Lewis, J.; Maroncelli, M. *Chem. Phys. Lett.* **1999**, *310*, 485.
(25) A similar study of more limited scope was also recently undertaken by Otomo and Koda.[41]
(26) Knutson, B. L.; Tomasko, D. L.; Eckert, C. A.; Debenedetti, P. G.; Chialvo, A. A. *Local Density Augmentation in Supercritical Solutions: A Comparison Between Fluorescence Spectroscopy and Molecular Dynamics Results*. In *Recent Advances in Supercritical Fluid Technology: Applications and Fundamental Studies*; Bright, F. V., McNally, M. E. P., Eds.; ACS Symposium Series; American Chemical Society: Washington, DC, 1992; Vol. 488; p 60.
(27) O'Brien, J. A.; Randolph, T. W.; Carlier, C.; Ganapathy, S. *AIChE J.* **1993**, *39*, 1061.
(28) deGrazia, J. L.; Randolph, T. W.; O'Brien, J. A. *J. Phys. Chem. A* **1998**, *102*, 1674.
(29) Adams, J. E. *J. Phys. Chem. B* **1998**, *102*, 7455.
(30) Frankland, S. J. V.; Maroncelli, M. Unpublished results, 1998.
(31) Frankland, S. J. V.; Maroncelli, M. *J. Chem. Phys.* **1999**, *110*, 1687.
(32) Patel, N.; Maroncelli, M. Unpublished results, 1999.
(33) Patel, N.; Frankland, S. J. V.; Maroncelli, M. Computer Simulations of Supercritical Solvation: Coumarin 153 in CO_2 and Ethane. Manuscript in preparation, 2000.
(34) Yonker, C. R.; Smith, R. D. *J. Phys. Chem.* **1988**, *92*, 235.
(35) Yee, G. G.; Fulton, J. L.; Smith, R. D. *J. Phys. Chem.* **1992**, *96*, 6172.
(36) Sun, Y.-P.; Fox, M. A.; Johnston, K. P. *J. Am. Chem. Soc.* **1992**, *114*, 1187.
(37) Bennett, G. E.; Johnston, K. P. *J. Phys. Chem.* **1994**, *98*, 441.
(38) Rice, J. K.; Niemeyer, E. D.; Dunbar, R. A.; Bright, F. V. *J. Am. Chem. Soc.* **1995**, *117*, 5832.
(39) Pan, X. Solute−Solvent Interactions and Raman CH Stretching Spectra of Cyclopentane-D9 and Cyclohexane-D11: Bridging the Vapor-Liquid Density Gap. Ph.D. Thesis, Duke University, Durham, NC, 1995.
(40) Schwarzer, D.; Troe, J.; Zerezke, M. *J. Chem. Phys.* **1997**, *107*, 8380.
(41) Otomo, J.; Koda, S. *Chem. Phys.* **1999**, *242*, 241.
(42) Pan, X.; McDonald, J. C.; MacPhail, R. A. *J. Chem. Phys.* **1999**, *110*, 1677.
(43) Bulgarevich, D.; Sako, T.; Sugeta, T.; Otake, K.; Takebayashi, Y.; Kamizawa, C.; Uesugi, J.; Kato, M. *J. Chem. Phys.* **1999**, *111*, 4239.
(44) Myers, D. J.; Shigeiwa, M.; Fayer, M. D.; Cherayil, B. J. *J. Phys. Chem. B* **2000**, *104*, 2402.
(45) Kanakubo, M.; Aizawa, T.; Kawakami, T.; Sato, O.; Ikushima, Y.; Hatakeda, K.; Saito, N. *J. Phys. Chem. B* **2000**, *104*, 2749.
(46) A number of authors have discussed how best to define local densities. See, for example, the discussions in refs 5, 12, and 19.
(47) This excess density can be readily appreciated from the fact that radial distribution functions of net solvent density typically peak at values of 2−3 under liquidlike conditions.
(48) The difference in density of the supercritical reference state is partially mitigated by the fact that supercritical solvents are at temperatures near to T_c, whereas room-temperature solvents are at much lower reduced temperatures, $T/T_c = 0.5-0.6$. The higher temperature of the supercritical reference state should make attractive interactions of lesser importance at these densities than in liquid solvents, and thus render the two reference states more similar than they would be otherwise.
(49) Heitz, M. P.; Maroncelli, M. *J. Phys. Chem. A* **1997**, *101*, 5852.
(50) It is also the case that $R(\epsilon)$, where ϵ is the dielectric constant, is nearly proportional to density, at least at low densities in supercritical fluids. Thus, to the extent that dielectric continuum expressions such as eq 4 represent the behavior of electronic shifts, one often predicts a proportionality between such shifts and effective local densities. We also note that in quadrupolar solvents such as CO_2, if electrical interactions are important for determining the spectral shift, dielectric continuum models such as the one embodied in eq 4 are not applicable. But here too it is reasonable to expect that in many cases the spectral shift will be linear in density.[22] Thus, in collecting experimental data from the literature, if local densities could not be derived by a more complete analysis, we assume that $\rho_{\text{eff}}{}^{\nu} \propto (\nu_{\text{obs}} - \nu_0)$ and set the proportionality constant using the assumption that $\rho_{\text{eff}}{}^{\nu} = \rho$ for $\rho = 2\rho_c$.
(51) Mason, E.; Spurling, T. *The Virial Equation of State*; Pergamon Press: Oxford, 1969.
(52) Shoup, D.; Szabo, A. *Biophys. J.* **1982**, *40*, 33.
(53) There are four systems among those studied for which the maximum of $g_{ij}(r)$ is less than this value of 2. (Here the maximum values are ~1.8.) In these cases we use the excellent correlation between K_{ij} and B_{ij} to estimate K_{ij}.

(54) This expression is the equivalent of the more familiar expression for the case of molecules *i*, *j* interacting via a spherically symmetric potential

$$U_{\mathrm{solv},i}/\rho_j = 4\pi\int_0^\infty g_{ij}(r)u_{ij}(r)r^2\mathrm{d}r$$

(55) There is still some "orientational" broadening of $g_{ij}^{ss}(s)$ due to the dispersion of solvent atom distances relative to the solvent's center of mass. The broadening is much smaller than that present in $g_{ij}^{0}(r)$ because the solvent molecules are more compact than the solutes. One could define distribution functions in terms of atom−atom distances to eliminate most of this source of broadening. We choose not to do so here because the distance *s* is the most direct indicator of whether a solvent molecule should be considered to be in the first solvation shell of the solute, and it is the energetics of such solvent−solute contacts that we wish to measure.

(56) The only difference is that in some simulations the intermolecular potential function is actually truncated at some cutoff radius, whereas in the 2-molecule calculations performed here, no truncation is applied.

(57) AMPAC5.0. Semichem Inc.: Shawnee, KS, 1994.

(58) Frisch, M. J.; Trucks, G. W.; Schlegel, H. B.; Gill, P. M. W.; Johnson, B. G.; Robb, M. A.; Cheeseman, J. R.; Keith, T.; Petersson, G. A.; Montgomery, J. A.; Raghavachari, K.; Al-Laham, M. A.; Zakrzewski, V. G.; Ortiz, J. V.; Foresman, J. B.; Cioslowski, J.; Stefanov, B. B.; Nanayakkara, A.; Challacombe, M.; Peng, C. Y.; Ayala, P. Y.; Chen, W.; Wong, M. W.; Andres, J. L.; Replogle, E. S.; Gomperts, R.; Martin, R. L.; Fox, D. J.; Binkley, J. S.; Defrees, D. J.; Baker, J.; Stewart, J. P.; Head-Gordon, M.; Gonzalez, C.; Pople, J. A. GAUSSIAN94; Gaussian, Inc., Pittsburgh, PA, 1995.

(59) Jorgensen, W. L. *BOSS*, version 4.0; Yale University: New Haven, CT, 1998.

(60) Jorgensen, W. L.; Maxwell, D. S.; Tirado-Rives, J. *J. Am. Chem. Soc*. **1996**, *118*, 11225.

(61) Dymond, J.; Smith, E. *The Virial Coefficients of Pure Gases and Mixtures*; Clarendon Press: Oxford, 1980.

(62) van der Hoef, M. A.; Madden, P. A. *J. Chem. Phys.* **1999**, *111*, 1520.

(63) Allen, M. P.; Tildesley, D. J. *Computer Simulation of Liquids*; Oxford: Oxford, 1987.

(64) Monson, P. A.; Rigby, M.; Steele, W. A. *Mol. Phys*. **1983**, *49*, 893.

(65) Freeman, D. *J. Chem. Phys*. **1975**, *62*, 4300.

(66) Dewar, M. J. S.; Zoebisch, E.; Healy, E.; Stewart, J. *J. Am. Chem. Soc*. **1985**, *107*, 3902.

(67) An exception is the study by Schwarzer and co-workers,[40] who performed thorough Monte Carlo simulations of the effects of density augmentation on vibrational relaxation. Their data were not included because the potential functions used were not of the Lennard−Jones type and because we could not translate the contact values of g(σ) measured in that work into local densities.

(68) There has been a great deal of interest in computer simulations of ions in supercritical water. See, for example, Flanagin, L. W.; Balbuena, P. B.; Johnston, K. P.; Rossky, P. J. *J. Phys. Chem. B* **1997**, *101*, 7998, and references therein.

(69) The filled point at zero density in the bottom cufod panel is the exact value at zero density, obtained from integration of $g(r) = \exp\{-u(r)/k_BT\}$. This value (2.86) differs from the value (2.3) given by the authors of ref 28, for unknown reasons.

(70) Different authors employ slightly different definitions of the first solvation shell, but our studies show that the results are not terribly sensitive to the choice, as long as only the nearest neighborhood of the solute is sampled.

(71) Urdahl, R. S.; Myers, D. J.; Rector, K. D.; Davis, P. H.; Cherayil, B. J.; Fayer, M. D. *J. Chem. Phys*. **1997**, *107*, 3747.

(72) For some of the single-site solute/solvent combinations, the coordination numbers and solvation energies were not provided in the original sources. However, we found that they could be reproduced with good accuracy (at least at $\rho = 2\rho_c$) using radial distribution functions from Percus−Yevick integral equation calculations.

(73) Bevington, P. R. *Data Reduction and Error Analysis for the Physical Sciences*; McGraw-Hill: New York, 1969.

(74) This statement is not strictly correct in the sense that our definition of effective density incorporates a dense fluid reference value. For example, consider spherically symmetric potentials. Here, one expects the value of $(\rho_{\mathrm{eff}}/\rho)_0$ to be proportional to the maximum value of $g_{uv}^{0}(r) = \exp(-u_{uv}(r)/k_BT)$, which is purely a function of u_{uv}. However, our normalization is equivalent to defining $(\rho_{\mathrm{eff}}/\rho)_0 \cong g_{uv}^{0}(r_{\max})/g_{uv}^{\mathrm{ref}}(r_{\max})$, where $g_{uv}^{\mathrm{ref}}(r)$ is the radial distribution function at the reference state, which depends in a complicated way on both $u-v$ and $v-v$ interactions in the dense fluid. We note that one might anticipate that normalization by $g_{uv}^{\mathrm{ref}}(r_{\max})$ might destroy any hope of correlating $(\rho_{\mathrm{eff}}/\rho)_0$ to pair-potential properties alone. However, in the simulated systems we have examined, $g_{uv}^{\mathrm{ref}}(r_{\max})$ does not vary greatly: a value of $2.5 \pm 0.5(1\sigma)$ is found for a wide variety of systems.

(75) We take 14 (out of 16) simulations, the number of distinct solute/solvent combinations, to be the size of the "independent" data set examined. Similarly, for the experimental data set we take the number of independent points to be 38 (out of the 52 data sets listed in Table 5).

(76) We also examined correlations in which only systems in the same supercritical solvent (CO_2, ethane, fluoroform) are compared. No significant differences were found for such single-solvent correlations compared to what is observed with the complete set of experimental data.

(77) For completeness we examined multiple linear regressions between the augmentation measures and the various quantities listed in Table 6. These multiple regressions did not provide significant improvements over the best single-variable correlations already discussed.

(78) Martinez, H. L.; Ravi, R.; Tucker, S. C. *J. Chem. Phys*. **1996**, *104*, 1067.

(79) Goodyear, G.; Tucker, S. C. *J. Chem. Phys*. **1999**, *111*, 9673.